

January 01, 2010

## Multi-scale replication of small intestine basement membrane via chemical vapor deposition

Brian Jarrett McMahon  
*Northeastern University*

---

### Recommended Citation

McMahon, Brian Jarrett, "Multi-scale replication of small intestine basement membrane via chemical vapor deposition" (2010). *Chemical Engineering Master's Theses*. Paper 11. <http://hdl.handle.net/2047/d20001043>

This work is available open access, hosted by Northeastern University.

**Multi-scale Replication of Small Intestine Basement Membrane via  
Chemical Vapor Deposition**

A Thesis Presented

by

Brian Jarrett McMahon

to

The Department of Chemical Engineering

in partial fulfillment of the requirements  
for the degree of

Masters of Science

in

Chemical Engineering

Northeastern University  
Boston, Massachusetts

November 23, 2010

## ACKNOWLEDGEMENT

I would like to express my deepest gratitude to my advisor Prof. Rebecca Carrier for her constant support, valuable insight, helpful advice, and patience throughout my graduate research. I would also like to thank the members of my thesis committee: Professor Daniel Burkey, for his expertise, helpful advice, and continued support through everything and Professor Shashi Murthy, for finding time in his busy schedule to provide feedback and helpful insights. I am also grateful to current and former lab mates: Fulden Buyukozturk, Stephanie Fernandez, Ece Gamsiz, Sean Kevlahan, Selena Di Maio, Narine Malkhasayan, Anna Poehler, Courtney Pfluger, Kyle Stephens, Lin Wang, and Hasan Yildiz, for their laboratory help, helpful conversations, and companionship along the journey. I would also like to thank James Green and Mariam Ismail for providing helpful distractions and reminding me that there is life outside of work. I would like to acknowledge Professor Al Sacco and the CAMMP Laboratory, Professor Katherine Ziemer and the Interface Engineering Lab, and Professor Max Diem for the use of their equipment. I would like to acknowledge Bill Fowle and the EM Laboratory for his helpful advice on biological fixation as well as the use of their equipment. I would like to acknowledge Rob Eagan for his expertise and his continuing willingness to help. I would like to thank my family for their continued support and encouragement in all that I do. The extent of this work was funded through a grant from the National Science Foundation, with which, this work would not have happened. Lastly, I would like to thank the Chemical Engineering Department at Northeastern University for the opportunity to conduct this research and grow as an engineer.

## ABSTRACT

In 2010, oral drug delivery was a \$49 billion industry. The major portal for the uptake of medicines delivered orally is the small intestine. One of the greatest features of the small intestine is the large surface area, created by an intricate structure of finger-like projections called villi and well-like invaginations called crypts. To help predict bioavailability of rapidly developed candidate drug compounds, cell culture models are frequently used. However, these tests are often inaccurate. It is hypothesized that the lack of cell culture substrate biochemistry and topography are major factors in the difference in cell function between *in vivo* and *in vitro* transport studies.

Chemical vapor deposition (CVD) provides the capability of recreating the intestinal basement membrane topography; it has been used to deposit silica coatings which have been shown to exactly replicate complex three-dimensional biological structures as small as 150 nm. Also, plasma enhanced CVD (PECVD) has been used to deposit a biocompatible, biodegradable polymer, poly(2-hydroxyethyl methacrylate) (pHEMA), with tunable amounts of cross-linking. However, literature reports that photoinitiated CVD (piCVD) produces a more chemically pure pHEMA film than PECVD.

It was found that the basement membrane of a porcine small intestine could be uncovered through an aldehyde-based fixation and maceration. CVD silica was then utilized to deposit a thin conformal layer upon the basement membrane. The silica was seen to replicate the villus and crypt structure on the order of 100  $\mu\text{m}$  and pores, on the surface of the villi, on the order of 5  $\mu\text{m}$ . However, it was found that sphere-like

nanostructures masked the fibrous makeup of the basement membrane at the 100 nm scale.

piCVD was utilized to deposit pHEMA films of varying degrees of cross-linking. It was found that the degree of cross-linking affected the degree to which films swelled and degraded, with the cross-linked films having the least amount of water uptake and maintaining film thickness over a 21 day incubation. It was also found that after 3 days the cross-linked films exhibited relative cell attachment equal to that of polystyrene, the industry norm, whereas the non cross-linked films showed 50% attachment.

## TABLE OF CONTENTS

LIST OF FIGURES .....	vii
LIST OF TABLES .....	viii
<b>1.0 Introduction</b> .....	1
<b>2.0 Critical Literature Review</b> .....	5
<b>2.1 Influence of Topography on Cellular Function</b> .....	5
2.1.1 Cell Adhesion.....	5
2.1.2 Cell Alignment.....	6
2.1.3 Gene Expression.....	7
2.1.4 Cell Morphology.....	8
<b>2.2 Methods of Creating Topography</b> .....	8
2.2.1 Random Surface Features.....	9
2.2.2 Laser Machining .....	10
2.2.3 Electro-spinning .....	11
2.2.4 Photolithography .....	12
2.2.5 Decellularized Natural Materials .....	13
<b>2.3 Chemical Vapor Deposition</b> .....	15
2.3.1 Materials Able to be Deposited.....	15
2.3.2 Initiation Methods.....	16
2.3.2.1 <i>Plasma Enhanced Chemical Vapor Deposition</i> .....	16
2.3.2.2 <i>Initiated Chemical Vapor Deposition</i> .....	19
2.3.2.4 <i>Photoinitiated Chemical Vapor Deposition</i> .....	21
<b>2.4 Characterization Methods to Analyze Biomaterials</b> .....	22
2.4.1 Variable Angle Spectroscopic Ellipsometry .....	22
2.4.2 Fourier Transform Infrared Spectroscopy .....	24
<b>3.0 Experimental</b> .....	28
<b>3.1 Introduction of Topography</b> .....	29
3.1.1 Small Intestine Preparation and Fixation.....	29
3.1.2 Chemical Vapor Deposition of Silica.....	30
<b>3.2 Introduce Biocompatible Materials</b> .....	31
3.2.1 Photoinitiated Chemical Vapor Deposition of pHEMA .....	31
3.2.2 Swelling and Degradation Characterization .....	32
3.2.3 Biocompatibility Study .....	33
3.2.4 Statistical Significance .....	34
<b>3.3 Characterization Methods to Analyze Biomaterials</b> .....	34
3.3.1 Spectroscopic Ellipsometry .....	35
3.3.2 Fourier Transform Infrared Spectroscopy .....	35
3.3.3 X-ray Photoelectron Spectroscopy .....	36
3.3.4 Scanning Electron Microscopy .....	37
3.3.5 Energy Dispersive X-ray Spectroscopy.....	38
<b>4.0 Results and Discussion</b> .....	39
<b>4.1 Small Intestine Preparation and Fixation</b> .....	39
<b>4.2 Chemical Vapor Deposition (CVD) of Silica</b> .....	40
4.2.1 Small Intestine Replication via CVD Silica .....	43
4.2.2 CVD Process Parameter Variation .....	46

<b>4.3 Photoinitiated Chemical Vapor Deposition (piCVD) of Biomaterial</b> .....	48
<b>4.3.1 piCVD of Non Cross-linked pHEMA</b> .....	49
<b>4.3.2 Cross-linking of pHEMA with Ethylene Glycol Diacrylate (EGDA)</b> .....	52
<b>4.3.3 Hydrogel Formation and Degradation of Non, Low, and High Cross-linked pHEMA</b> .....	55
<i>4.3.3.1 Film Swelling</i> .....	56
<i>4.3.3.2 Film Degradation</i> .....	58
<b>4.3.4 Cell Attachment Study</b> .....	59
<b>5.0 Conclusions</b> .....	62
<b>6.0 Recommendations</b> .....	64
<b>7.0 References</b> .....	66

## LIST OF FIGURES

Figure 1: SEM images of the naked small intestine basement membrane depicting the multi-scale topography intended to be replicated. ....	40
Figure 2: FTIR spectra of a silica film deposited on silicon wafer.....	41
Figure 3: SEM images of uncoated (a, c, e) and silica coated (b, d, f) porcine intestine basement membrane.....	44
Figure 4: EDS spectrum of the a) uncoated and b) silica coated intestinal basement membrane. Note that the large Si peak that appears on the sample that has undergone the silica deposition step, as opposed to the C-dominated spectrum for the native tissue.....	45
Figure 5: FTIR spectra of the final silica deposition optimization showing the positive effect of lowering overall flow rate into the reactor. ....	47
Figure 6: FTIR spectra showing the dramatic lowering of hydroxyl in the silica film after a gentle post deposition annealing process. ....	48
Figure 7: FTIR spectra of non cross-linked pHEMA illustrating the retention of chemical constituencies from the liquid monomer.....	49
Figure 8: XPS oxygen 1s atomic spectra with de-convoluted peaks for non cross-linked pHEMA films.....	51
Figure 9: FTIR spectra exhibiting the incorporation of chemical cross-linker. The inverse variation of hydroxyl and carbonyl peak intensity is due to EGDA having no –OH and two C=O groups. ....	52
Figure 10: XPS oxygen 1s atomic spectra with de-convoluted peaks for a) non, b) low, and c) high cross-linked pHEMA films. The relative loss of hydroxyl area under the de-convoluted peak confirms the incorporation of EGDA. ....	54
Figure 11: Film thickness increase as a function of cross-linking after 24 hours in solution. High error in non cross-linked films is due to 40% overall thickness loss after 24 hours. ....	57
Figure 12: Degradation profiles as a function of cross-linking over a 21 day time period. Non cross-linked films retained integrity after an initial thickness loss. Cross-linked films retain thickness throughout the duration of the study. (*) indicates statistical significance compared to cross-linked films ( $p < 0.0005$ ).....	58
Figure 13: Relative cell attachment on thin films compared to polystyrene after 3 day cell culture. Cross-linking shows improved cell attachment when compared to non cross-linked films. (*) indicates statistical significance compared to polystyrene and the cross-linked films ( $p < 0.05$ ).....	60

## LIST OF TABLES

Table 1: FTIR peak assignments for organic and organosiloxane films .....	27
Table 2: High resolution XPS scan data for de-convolution peak fitting .....	37

## 1.0 Introduction

The oral drug delivery market is presently valued, in 2010, as a \$49 billion industry, and is expected to grow 11.3% per year.<sup>1</sup> This market continues to control the majority of the drug delivery industry due to ease of administration. Growth of the market, however, will be driven by newer technologies allowing for controlled release as well as new oral formulations of drugs previously available only in injectable forms. Innovative oral delivery methods such as orally disintegrating tablets, fast dissolving tablets and mini-tablets have been introduced into the market, which ensure better patient compliance, reduce dosage frequencies, and enable customizable drug loading.<sup>1</sup>

The major portal for the uptake of orally delivered medicines is the small intestine. The small intestine consists of three distinct sections: duodenum, jejunum, and ileum.<sup>2</sup> The duodenum is the first section of the small intestine and is approximately 10 inches in length. The principle function of the duodenum is chemical digestion and neutralization of stomach acids. The jejunum, the second section of the small intestine, is approximately 9 feet in length. The jejunum is responsible for the majority of nutrient and compound absorption. The ileum, the third and final section of the small intestine, is approximately 13 feet in length. The ileum functions primarily to absorb vitamin B<sub>12</sub> and reabsorb bile salts.

One of the defining features of the small intestine is its large surface area. The basement membrane of the small intestine consists of an intricate invaginated structure with features at many different scales. Macroscopic folds, millimeters in scale, create increased surface area which helps to slow passage through the intestine. On the surface of these folds, finger-like projections called villi and invaginations called crypts, both

100's of micrometers in scale, further increase the surface area. The surface of the intestinal basement membrane possesses pores approximately 1-5  $\mu\text{m}$  in diameter. Finally, at the nanometer-scale, fibrous materials in an interwoven pattern provide the ultra-structure of the extracellular matrix (ECM). The intestinal epithelium grows upon the surface of these villi and crypts. The intestinal epithelium consists of many different cell types including: enterocytes, goblet, paneth, and undifferentiated cells.<sup>2</sup> Enterocytes, tall columnar cells with microvilli further increasing surface area, are responsible for most absorption. Goblet cells are responsible for mucus secretion. Paneth cells are responsible for the regulation of intestinal bacteria. Undifferentiated cells, stem cells, are found only in crypts and give rise to all other cells in the intestine.

When new drug compounds are developed by pharmaceutical companies, bioavailability tests must be conducted to determine if the drug will be absorbed into the body at a desirable amount. Typically, two different approaches are available for these studies; animal models and cell cultures. Animal studies, in addition to their ethical issues, have multiple drawbacks. First, these studies can be extremely expensive and time consuming as the test subjects have to be raised to suitable ages before being used. Also, to determine the extent to which the drug is available throughout the body, the subject is euthanized, allowing for single-use only. Finally, it has also been found that animal studies are not always an acceptable representation of how a drug may be absorbed into a human body.<sup>3</sup>

Cell cultures are typically carried out using flat porous substrates. Cells are grown to a confluent layer upon the substrate. A compound is then dosed into the apical compartment and measurements are taken over time from the basolateral compartment to

determine the transport across the cell layer.<sup>4</sup> These cultures typically use human Caco-2 cells as an *in vitro* model.<sup>5</sup> These cells, though derived from a colon cancer line, are believed to differentiate into a similar phenotype as enterocytes and are a suitable analog to small intestinal epithelium.<sup>6</sup> These studies, however, use flat substrates as well as chemistries which are not seen within the body.

Extensive research has been conducted in an effort to introduce topography to cell populations. These studies have focused on creating analog substrates for cell culture, usually regular, single-scale surface features. Typical analog features consist of random features,<sup>7,8</sup> fibers,<sup>9,10</sup> channels,<sup>11,12</sup> or posts and wells.<sup>13</sup> For example, increased random surface roughness via sandblasting increased gene expression and mineralization in cultured osteoblasts.<sup>14</sup> Grooves of varying depth, width and frequency have also been shown to induce cells to orientate themselves with respect to the grooves.<sup>15</sup> Nanofibrillar matrixes created by electrospinning a polymer solution produced kidney cells with morphologies and characteristics of cells found *in vivo*, as well as breast epithelial cells that underwent morphogenesis to create multicellular spheroids containing lumens.<sup>16</sup> Recent work, however, has shown the efficacy of using actual extra cellular matrix as a cell culture substrate. It was seen that an entire rat heart<sup>17</sup> and nerve grafts<sup>18</sup> were able to be completely decellularized. The rat heart was then able to be recellularized and demonstrated that, due to retention of the complex cardiac structure and through maturation of the cells, pump function could be accomplished. Also, the nerve graft was implanted between pieces of severed nerve and demonstrated no difference significant immunological response. These results suggest that culturing cells on biomimetic constructs that replicate complex, irregular *in vivo* topography as fully as possible may

induce a phenotype that resembles that of cells *in vivo* to a much greater extent than culture on flat, non-mimetic substrates.

Chemical vapor deposition (CVD) provides an opportunity to precisely replicate multi-scale irregular features. CVD is a polymerization technique that utilizes delivery of vapor-phase monomers to form chemically well-defined films on the surface of substrates. CVD has a long history in the semiconductor processing industry as a methodology for creating thin, conformal coatings on substrates that exhibit a three-dimensional topography at the micro- and nanoscales.<sup>19,20</sup> Many of the topographical features of native biological tissue, and the intestinal basement membrane in particular, are microns or tens-to-hundreds of microns in scale – easily within the scope of CVD coating process capabilities. CVD is able to provide a conformal coating that is challenging for traditional wet chemical processes, primarily because CVD is a solvent free, vapor-phase process, and as such avoids many solvent-related issues, such as wetting, surface tension effects, and fluid flow issues at small length scales. The most enticing properties of CVD are the low-energy input to drive selective chemistry, modest vacuum, and room-temperature conditions which make it compatible with sensitive substrates.<sup>20</sup> Furthermore, CVD has been shown to have the ability to deposit biocompatible polymeric coatings for a variety of applications, such as coatings for neural probes, cell culture, controlled release of drugs, and biosensors.<sup>21,22</sup> Thus, CVD provides the opportunity to create biocompatible substrates with biomimetic topographies for use as cell culture substrates.

## 2.0 Critical Literature Review

The small intestine has a large surface area due to its invaginated structure. The basement membrane of the small intestine, upon which the epithelial cells grow, consists of topographies at multiple scales. These topographies range from millimeter sized folds to nanoscale fibrous material. However, when intestinal cells are cultured for drug transport studies, the cells are grown upon substrates with flat topographies. It is thought that one of the major differences between *in vitro* models and *in vivo* studies is that the lack of topography creates phenotypes not seen in the body. Since the focus of this study is the multi-scale replication of the small intestine, it is important to learn about the extent to which cells respond to topography, methodologies for introducing topography, and to what extent chemical vapor deposition can be utilized, in order to accomplish our goals.

### 2.1 Influence of Topography on Cellular Function

Topography has recently attracted a lot of interest with respect to cell culture substrates. Studies have focused on the effect of topography on adhesion, alignment, gene expression, and morphological changes. However, these studies have typically focused on regular, single-scale features. It is, therefore, necessary to understand the effect that irregular, multi-scale features may have on cellular response.

#### 2.1.1 Cell Adhesion

Cell adhesion is an important aspect of many physiological processes, including tissue development and maintenance, cell migration, and wound healing. A major cellular component participating in cell adhesion is focal adhesions (FA). FAs, having been observed as early as 1964,<sup>23</sup> consist of two different types of proteins, signaling and structural. Signaling proteins, including focal adhesion kinase (FAK), have been shown

to have the ability to act as mechanosensors, sensing and responding to local forces.<sup>24</sup> Structural proteins such as paxillin have been shown to respond differently to varying topographies.<sup>25</sup> For example, when human foreskin fibroblasts (HFF) were cultured on varied nanoscale topographies, cells cultured on nanopost surfaces exhibited similar dot-like paxillin patterns as cells on smooth surfaces. However, cells cultured on nanograting presented elongated patterns. Vinculin, another structural protein, has also been shown to be induced in response to nanoscale substrate topography.<sup>26</sup> For example, human epithelial cervical cancer (HeLa) cells cultured on substrates with different microscale topographies, and cells cultured on micropit substrates showed an increased vinculin expression. However, no increase was seen when comparing cells cultured on etched irradiated substrates to cells cultured on unetched substrates and etched unirradiated substrates. In another study, human fetal osteoblast (hFOB) cells exhibited significantly greater cell attachment when cultured on shallow nanopit surfaces compared to flat substrates.<sup>7</sup> However, cell attachment decreased with increasing pit depth. This result seems counterintuitive, but indicates that these cells prefer some surface roughness rather than deep wells for attachment. There were also differences in FAK, paxillin and vinculin expression in cases of enhanced cell attachment, demonstrating increased expression on nanopit surfaces compared to flat substrates.<sup>7</sup>

### **2.1.2 Cell Alignment**

Organized alignment of cells is critical to controlling tissue microarchitecture and biological function. The importance of substrate topography to alignment of cell populations has been supported by multiple studies. It has been shown that cells will align with simple microgrooves.<sup>15</sup> For example, melanocytes, a type of skin cell, aligned

their elongated axis parallel to the grooves. In contrast, cells cultured upon flat substrates showed no orientation. An increase in height and frequency of the grooves caused a stronger orientation response from the cells. The influence of width and depth of microgrooves on keratinocytes, dermal cells, was also examined.<sup>11</sup> These cells created a continuous epidermis-like structure on grooved substrates after 10 days in culture. It was also found that the cells preferred the channels with an increased stratification and alignment of cells within the channels as the channel depth became greater.

### **2.1.3 Gene Expression**

Cellular function requires the production and use of many different types of proteins. In order for cells to make the proteins required for cell function, different genes must be expressed within the cell. It is believed that topographical cues may influence gene expression in many different types of cells. For example, fibroblasts exhibit differing gene expression on flat surfaces compared to grooved surfaces.<sup>27</sup> After an initial 24 hours on the grooves, the cells up-regulated cell signaling genes. However, after 5 days, the cells exhibited a down-regulation of many of the same genes, demonstrating the temporal dependence of response to topography. It was concluded that topography has an overall effect on DNA transcription and thus, protein translation. In another study, it was found that after 21 days, cells cultured on the hexagonally arranged nanopits had broad down-regulation of genes when compared to cells cultured on flat substrates.<sup>28</sup> It was proposed that nanotopography can affect adhesion and differentiation which may in turn influence gene transcription. Furthermore, it was postulated that direct mechanical linking with an underlying matrix may lead to gene positioning and, therefore, regulation, specifically of adhesion proteins.

#### **2.1.4 Cell Morphology**

Cells have been known to exhibit many different shapes and structures. The morphology that cells exhibit can be indicative of the overall health of the cells or the state of differentiation. Topography has been shown to influence cell morphology and subsequently the differentiation of neural stem cells.<sup>10</sup> It was found that cells elongated along the axis of aligned fibers and extended neurites guided along the axis of the fibers when compared to random extension on randomly oriented fibers. Mardin-Darby canine kidney (MDCK) epithelial cells cultured on smooth substrates were round, while cells cultured on nanogrooved substrates showed improved spreading and enhanced alignment of actin filaments when cultured on nanogrooved substrates.<sup>12</sup> Mouse embryonic fibroblast (3T3) cells cultured on pillar substrates exhibited more branching when compared to cells on flat substrates.<sup>29</sup> It appeared that a key mechanism for guiding cell migration was the extension of these long protrusions. Cells also exhibited different morphologies depending upon the spacing between the pillars. HFF cells exhibited different morphologies when cultured on substrates with varied nanoscale topographies.<sup>25</sup> It was found that cells cultured on nanopost surfaces exhibited rounded morphologies and appeared smaller, while cells cultured on nanogratings were elongated. Morphologies on both surfaces varied significantly from those of cells grown on smooth substrates, which were spread with a flattened morphology.

#### **2.2 Methods of Creating Topography**

In an effort to more closely mimic *in vivo* conditions, many different methods to create substrates with specific topographies have been explored. A wide variety of features including random features (e.g., surface roughness), grooves, ridges, fibers, posts

and wells have been explored. Typical methods of creating these features consist of random placement, laser machining, electro-spinning, lithography, and decellularization of natural materials. Examples of these different methods being used to create substrates useful for cell culture are described below.

### **2.2.1 Random Surface Features**

There are a variety of methods for creating random surface feature, including manual placement (e.g., using sandpaper) or variation of processing parameters. Lim and coworkers produced random nanoscale topographies via polymer demixing.<sup>7</sup> A 50/50 w/w solution of poly(L-lactic acid) and polystyrene was used. To vary the depth of the random nanopits generated by the demixing process, the polymer solution was mixed with chloroform at different concentrations; 0.5, 1 or 1.5% w/w. The solutions were then spin-cast on glass cover slips to create thin films which were left to dry at room temperature with no further annealing. Atomic force microscopy was utilized to determine the depth of the nanopits created on the surface. It was found that increasing the amount of polymer in the solution led to deeper pits. However, pit depth exhibited wide variations: 0.5% solution resulted in depths of  $14.3 \pm 1.8$  nm, 1% solution resulted in depths of  $28.5 \pm 4.3$  nm, and 1.5% solution resulted in depths of  $45.3 \pm 4.7$  nm. These substrates present simple nanoscale topography which could be used to study effects on cell area and adhesion.

Sardella and coworkers produced random nanoscale topographies via plasma enhanced chemical vapor depositions of fluorocarbons.<sup>8</sup> This study focused on the concept of afterglow, where the plasma field can interact with the substrate depending upon distance from the source. If the substrate is located too close to the plasma source,

chemical reactions and ion interactions can lead to significant monomer fragmentation. Subsequently, as the substrate is moved further away from the plasma source, the polymer films deposited exhibit chemistry and structure similar to conventional means of preparation. This theory was used to deposit two different chemicals, hexafluoropropylene oxide and hexafluoropropylene, at three different distances, 1, 8, and 18 cm. Atomic force microscopy was utilized to determine the surface roughness of each film. It was found that the oxide films displayed increased surface roughness from  $1.1 \pm 0.2$  nm to  $426 \pm 52$  nm with increasing distance from 1 cm to 18 cm. The non oxide films showed the opposite affect, decreasing in surface roughness as distance increased. These substrates were then used to determine the effect of nano roughness on cell behavior and morphology.

### **2.2.2 Laser Machining**

There are many different ways to cut materials and create patterns. Laser cutting provides a method to reduce contamination and increase precision by utilizing a high energy beam directed by computers. Pins and coworkers produced surfaces with microgrooves of various widths and depths via laser machining.<sup>11</sup> Laser machining was used to create a master chip with grooves of widths and depths between 40 – 200  $\mu$ m. The laser beam was focused onto the surface and then pulsed to ablate the surface. The beam was then repositioned and pulsed again until all channels were created. Negative replicates were then cast from the microgrooved structure using polydimethylsiloxane (PDMS). Then, to create a basal lamina analog, gelatin or collagen were poured onto the negative PDMS mold to create culture substrates with grooves similar to the master chip. It was found, however, that this method of preparing substrates resulted in grooves with

widths and depths varying significantly from the specified dimensions. These substrates were used to determine the affect of width and depth of microgrooves on cell differentiation.

Jin and coworkers produced nanogrooves via laser irradiation.<sup>12</sup> Nanogrooves were produced in polystyrene tissue culture dishes by irradiating the surface with a pulse polarized UV-laser. The samples were fixed to a remotely controlled stand that allowed motion in the X and Y-directions. Atomic force microscopy was then utilized to determine the frequency and depth of the nanogrooves. It was found that the groove frequency could be controlled at a 300 – 400 nm range, where depth could be controlled by the incident angle of the laser. These substrates were then used to determine the effect of nanogrooves on cell adhesion and growth.

### **2.2.3 Electro-spinning**

There are a few ways to create fibers at a micro or nanoscale including electro-spraying and solution dry spinning. Electro-spinning differs from these methods by not requiring high temperatures which allows for the creation of fibers from large complex molecules. Cooper and coworkers produced nanofibers of varying orientation via electro-spinning.<sup>9</sup> A mixture of chitosan and polycaprolactone at a ratio of 40 : 60, respectively, was utilized. The mixture was gravity fed from a syringe toward a rotating drum to create randomly oriented fibers, or toward two grounded parallel electrodes to create aligned fibers. The fiber bundles were then attached to coverslips for cell culture. Scanning electron microscopy was utilized to determine the diameter and the exact orientation of the fibers. The fibers had diameters of  $175.82 \pm 55.95$  and  $215.79 \pm 44.2$  nm for the random and oriented types, respectively. In spite of the high variability in

diameter, the fibers were able to be aligned in a bundle when desired. These substrates were then used to determine how muscle cells would respond to the different fiber organizations.

Lim and coworkers produced nanofibers of varying orientation via electrospinning.<sup>10</sup> A mixture of polycaprolactone with octadecyl rhodamine B chloride was dispersed from a syringe pump onto a stationary grounded collector to create randomly oriented fibers, or onto a rotating disc collector to create aligned fibers. Scanning electron microscopy was utilized to determine the diameter and orientation of the fibers. It was found that fiber diameter could be changed from 260 to 930 nm by altering the concentration of the polymer solution from 12 to 14%, respectively. These results indicate the ability to tailor the thickness and orientation of nanofibers for a desired function. These substrates were then used to determine the effect guided alignment would have on differentiation of stem cells.

#### **2.2.4 Photolithography**

Lithography has been used for hundreds of years to reliably print images or text from a master plate. Recently, this method has been tailored to produce micro and nanoscale topographies through the use of light-sensitive photo resists and photo masks. Biggs and coworkers produced nanoscale groove and ridge arrays via photolithography.<sup>30</sup> A template of parallel slits was created by exposing a photoresist layer to a UV light through a chrome photomask. The substrate was then etched in gas plasma and stripped of photoresist. The substrate was then coated with a thin layer of Ni-V to act as the master. The master was then coated with poly(methyl-methacrylate) for use as a cell culture substrate. It was found that the grooves had depths of 330 nm and widths ranging

from 10 – 100  $\mu\text{m}$ . These substrates were then used to determine the effect of nanoscale grooves on cell organization and adhesion.

Wang and coworkers produced micro-wells via photolithography.<sup>13</sup> A template of multiple arrays of circles, with varying diameters, was printed with high resolution on a transparency. The transparency was then used as a photomask to create a master mold with micro-pillar features using UV lithography. Polydimethylsiloxane was then poured onto the micro-pillar array to create the micro-well patterned cell culture substrate. Scanning electron microscopy was utilized to analyze the topography of the cell culture substrates. It was found that the micro-wells had smooth side walls and bottoms, but that the diameter of the wells was not the same from top to bottom. The dimensions of the micro-wells were designed to enable micro-well arrays to provide an analog to typical crypt structures found in the intestine. These substrates were then used to determine the effect of crypt-like topography on cell morphology.

### **2.2.5 Decellularized Natural Materials**

Limited supply of donor organs and rejection of implants have led to the idea of creation of bioartificial organs. These implantable devices have focused on using actual extra cellular matrix for a scaffold upon which to develop tissues. Ott and coworkers decellularized heart extra cellular matrix via coronary perfusion with detergent.<sup>17</sup> An aortic cannula was inserted into a dissected rat heart to allow for coronary perfusion. Heparinized phosphate buffer solution containing adenosine was perfused for 15 minutes. A solution of 1% sodium dodecyl sulfate (SDS) in deionized water was then perfused for 12 hours. The heart was then rinsed by perfusing deionized water for 15 minutes, and further perfused with a 1% Triton X-100 solution for 30 minutes. A solution containing

antibiotics was then perfused through the heart to prepare the scaffold for cell culture. This structure was then recellularized with rat heart cells to determine whether the cells would be able to grow on the natural structure. This method provides a way to uncover the membrane upon which cells actually grow *in vivo*. However, this method does not allow for repeated use, and is extremely time consuming. It also remains to be determined to what extent the perfusion solutions are removed from the scaffold before cell culture occurs.

Hudson and coworkers decellularized nerve grafts via immersion of nerve tissue in detergent solutions.<sup>18</sup> Dissected rat sciatic nerves were immediately placed in solution and fatty and connective tissue was removed. The nerve was cut into pieces and placed in deionized distilled water for 7 hours. The water was then removed and replaced with a detergent solution, SB-10, and agitated for 15 hours. The tissue was then rinsed in a washing solution before being placed in a second detergent solution, Triton X-200, and agitated for 24 hours. The nerve was then rinsed again in washing solution before being placed again in the SB-10 solution for 7 hours, rinsed, and then placed in a final detergent solution, SB-15/Triton X-200, for 15 hours. Finally, the nerve was rinsed in the washing solution three times. This structure was then implanted into rats between two pieces of severed nerve to determine response to the decellularized nerve, including potential infiltration of nerve cells. This method provides a unique procedure for removing all cellular material from a nerve for implantation into the body for nerve regeneration. It was found that these materials could be surgically handled and implanted, and allowed regeneration of axons to a greater extent than freeze-thaw and chemically decellularized grafts.

## **2.3 Chemical Vapor Deposition**

Chemical vapor deposition (CVD) is a polymerization technique that utilizes delivery of vapor-phase monomers to form chemically well-defined films on the surfaces of substrates. CVD polymers are desirable as surface modification layers due to strong retention of organic functional groups and the ability to produce conformal coatings. The most enticing properties of CVD are the low-energy input to drive selective chemistry, modest vacuum, and room-temperature conditions, which make it compatible with sensitive substrates.<sup>20</sup>

### **2.3.1 Materials Able to be Deposited**

Chemical vapor deposition (CVD) has been utilized exhaustively in the semiconductor industry to produce silica-based materials for use as interconnect materials. It has been shown that at room temperature and relatively low vacuum (750 – 3750 mTorr), silane reacts with excess vaporized hydrogen peroxide to deposit silica.<sup>31</sup> Recently, this reaction has been repurposed as an effective way to coat delicate biological specimens.<sup>32</sup> Silane vapors were admitted with hydrogen peroxide at ratios between 1:10 and 1:30 into a CVD chamber containing a butterfly wing. All surfaces, in addition to the substrate, were coated at rates between 50 and 200 nm/min. In order to remove the biological template (butterfly wing) from the deposited silica mold, a calcination step (500 °C) was utilized. However, this resulted in an overall 25% reduction in features of the original specimen, as well as possible creasing and destruction.

In addition to inorganic depositions, the knowledge of solution-based polymerization combined with the need to incorporate the desired properties of CVD has led to the deposition of polymer films. Solution-based polymerization is comprised of

three steps: monomers reacting in liquid phase, film formation through varied techniques, and a curing step. CVD, in contrast, provides the opportunity to deposit conformal polymer films in a single, solvent-free step. The polymers that are deposited can have many different desired properties including: controlled surface energy and functionalization, electrical conductivity, pH-responsiveness, and temperature-responsiveness.<sup>20</sup> Hydrogels, which are highly useful in various biochemistry and bioengineering applications, have also been deposited via CVD. Hydrogels exhibit the ability to swell in the presence of water, can be comprised of biocompatible materials, and have the ability to be cross-linked. One of the most widely studied hydrogel-forming polymers able to be deposited via CVD is poly (2-hydroxyethyl methacrylate) (pHEMA).

### **2.3.2 Initiation Methods**

Chemical vapor deposition (CVD) utilizes many different methods of creating polymer films, including free-radical polymerization. Free radicals, consisting of an unpaired electron, are useful in CVD because of their high reactivity and short lifetimes. It is generally accepted that free-radical polymerization consists of three main steps: initiation, propagation, and termination.<sup>20</sup> Initiation, the creation of free radical species, typically occurs by exposing a separate chemical initiator to heat, light or a redox reaction. This radical then reacts with the desired monomer to create a radicalized species which is ready to propagate and create polymer chains. It has been found that poly (2-hydroxyethyl methacrylate) (pHEMA) can be deposited through free-radical polymerization with many different excitation sources including: plasma, chemical initiation, and UV light.

#### ***2.3.2.1 Plasma Enhanced Chemical Vapor Deposition***

Plasma enhanced chemical vapor deposition (PECVD) utilizes a plasma field created by a discharge of electrical charge between two electrodes. This plasma field causes excitation of the vapor phase and radicalizes species as they flow into the reactor. The degree to which species are radicalized can be changed by changing plasma power or the pulsing of excitation.<sup>20</sup>

Tarducci and coworkers produced PECVD pHEMA films and compared surface chemistry with conventional pHEMA films.<sup>33</sup> HEMA monomer was introduced into a glass reactor at a rate of  $4 \times 10^{-8}$  mol/s at a pressure of 75 mTorr. Two separate plasma experiments were conducted, pulsed and continuous wave plasma. Pulsed plasma consisted of 20  $\mu$ s time-on, 20 ms time-off, and 40 W peak power. Continuous wave plasma consisted of constant 3 W power. Both of the experiments were conducted for 15 minutes, and results were compared to a reference sample prepared via spin coating. By comparing X-ray photoelectron spectroscopy (XPS) elemental analysis, it was found that the pulsed plasma film resembled the conventionally prepared film, both being comprised of 68% carbon and 32% oxygen. This result compared favorably to the theoretical make up of a pHEMA film, 66.6% carbon and 33.3% oxygen. However, it was seen that the continuous wave sample exhibited severe depletion of the oxygen content, with carbon accounting for 76%. This work demonstrates that PECVD provides a viable method of depositing a biocompatible pHEMA film.

Pfluger and coworkers added a cross-linker, ethylene glycol diacrylate (EGDA), to PECVD pHEMA films in an effort to tailor hydrophilicity.<sup>34</sup> In addition to the cross-linker, the study used a chemical initiator, *tert*-butyl peroxide (TBPO), and a plasma initiator, argon. HEMA monomer (4 sccm for non-cross-linked and 6 sccm for cross-

linked films) flowed into a stainless steel reactor together with 1 sccm TBPO and 5 sccm argon at a pressure of 350 mTorr. The EGDA flow rate into the reactor was varied by changing the temperature to which the liquid monomer was heated: 42 °C for low cross-linking and 48 °C for high cross-linking. Plasma excitation was maintained constant at 20 W power. XPS elemental analysis demonstrated that this plasma film resembled the continuous wave film prepared by Tarducci, having carbon and oxygen make up around 78.9% and 21.1%, respectively. This result, however, does not compare favorably to the theoretical values for pHEMA. The difference can be attributed to the addition of a chemical initiator with a ratio of 3 carbon atoms to 1 oxygen atom, as well as the elevated plasma power. The increase in plasma power, from 3 W to 20 W, could have caused an overall loss in chemical structure due to the high level of excitation from the plasma. However, the study showed the incorporation of the cross-linker, EGDA, through an increase in the carbonyl peak in Fourier transform infrared spectra. The incorporation was further confirmed by a decrease in the area under the hydroxyl de-convoluted peak in the oxygen 1s XPS scan. These films were then used in swelling and degradation studies to determine to what extent the cross-linking affected the properties of the films. It was found that uncross-linked pHEMA films exhibited the greatest degree of swelling, while the high cross-linked films swelled the least. This result was expected, as a decrease in hydrophilic component of the pHEMA films, the hydroxyl group, would allow less permeation of water into the film. It was also found that the degree of cross-linking had an effect on the ability of the film to retain thickness over a 21 day aqueous incubation period, retaining 73% and 88% thickness for low and high cross-linked films,

respectively. The uncross-linked pHEMA film degraded completely after 7 days in solution.

Pfluger and coworkers also determined the extent to which these cross-linked films could be used as biocompatible substrates by conducting cell attachment and viability studies.<sup>35</sup> Identical reaction conditions as those described above were utilized to produce films of varying cross-linking densities. Caco-2 cells were then cultured on the surfaces of the low and high cross-linked materials, as well as polystyrene and poly(dimethylsiloxane) as controls. It was found that high levels of cross-linking increased the degree to which cells would attach to the surfaces. After day 3 in culture, there was no significant difference in cell number on the polystyrene, low, and high cross-linked substrates. These results, together with the fact that cell viability on these substrates did not drop below 85%, lead to the conclusion that cross-linked pHEMA films are suitable culture substrates. However, it should be noted that the Caco-2 cell line is known to be a rather robust cell population.

#### ***2.3.2.2 Initiated Chemical Vapor Deposition***

Initiated chemical vapor deposition (iCVD), a subset of hot filament CVD (HFCVD), utilizes an array of hot wires to decompose a chemical initiator. The chemical initiator is flowed into the reactor, with the desired monomer, and decomposes in the vapor phase creating free radicals. These radicals then initiate free-radical polymerization with the monomers adsorbed to the substrate. The use of a chemical initiator is an improvement over previous HFCVD methodology, because the wires used to be heated to excessive temperatures (500 °C) to radicalize the monomer. However, the

initiators typically consist of peroxides which are much more easily radicalized; requiring temperatures much lower (200 °C).

Chan and coworkers were able to produce high quality pHEMA films by utilizing the iCVD mechanism.<sup>36</sup> This comprehensive study used a chemical initiator, *tert*-butyl peroxide (TBPO), a carrier gas, nitrogen, and a cross-linking agent, ethylene glycol diacrylate (EGDA). HEMA flow rate into the reactor varied from 3 – 5 sccm for uncross-linked pHEMA films, and was held constant at 4 sccm for cross-linked films. TBPO flow rate into the reactor was held constant at 1 sccm for all experiments, while nitrogen flow rate was varied to maintain a total flow rate into the reactor of 7 sccm. Reactor pressure was maintained at 350 mTorr and the Nichrome filament array was maintained at 280 °C for all experiments. For comparison, a pHEMA standard was obtained and cast onto a silicon substrate. Fourier transform infrared spectra were compared for the iCVD and standard, and no differences were seen. X-ray photoelectron spectroscopy (XPS) elemental analysis was further utilized to show that the piCVD film resembled the conventionally prepared film, both having carbon and oxygen make up around 68% and 32%, respectively. It is further explained that the difference between these values and the theoretical pHEMA make up, 66.6% and 33.3%, can be attributed to inaccuracies in relative sensitivity factors. The conclusion is then drawn that because the chemical make ups of the films are near identical, the two films have the same atomic composition. The elemental XPS peaks were then de-convoluted to determine the relative amounts of each of the chemical constituent in the film. It was found that there were five carbon and three oxygen moieties, as expected. The binding energy and percent area of each of these moieties was found to be near identical to the pHEMA

reference. XPS analysis was also performed on the cross-linked films, confirming the incorporation of the cross-linker by a decrease in the area under the hydroxyl peak in the de-convoluted oxygen 1s scan. The conclusion is drawn that the amount of cross-linking in the films can be controlled by the partial pressure of the EGDA monomer in the reactor. These results demonstrate that iCVD is a viable method of creating thin conformal polymer films of varying amounts of cross-linking.

#### ***2.3.2.4 Photoinitiated Chemical Vapor Deposition***

Photoinitiated chemical vapor deposition (piCVD) utilizes an ultraviolet light source to selectively decompose a chemical initiator to form free radicals. The UV light provides photons at specific wavelengths which are known to radicalize specific chemical bonds. However, because piCVD does not involve plasma or high temperatures, it is a useful method for depositing films on sensitive materials.

Baxamusa and coworkers were able to produce high quality pHEMA films on sensitive substrates by utilizing the piCVD method.<sup>37</sup> HEMA monomer flowed into a stainless steel reactor at rates between 1 – 2.5 sccm at a pressure of 100 mTorr, and no separate photoinitiator was used. A low-power ultraviolet lamp was mounted above a quartz viewport, allowing for light to enter the reactor at a wavelength of 254 nm. It was determined that the intensity of the light on the substrate was 50  $\mu\text{W}/\text{cm}^2$ . For comparison, a pHEMA standard was obtained and spun-cast onto a silicon substrate. Fourier transform infrared spectra were compared for the piCVD and standard, and no differences were seen. It was also demonstrated, via a swelling study, that these films display the ability to reversibly swell when placed in solution. This study shows the ability to coat sensitive substrates, such as biological sensors, with biomaterials which

allow for transport of small molecules. However, the study does not examine the long-term durability of these films. Also, no study has been done similar to that of Chan et al.,<sup>36</sup> testing the ability to cross-link these films.

## **2.4 Characterization Methods to Analyze Biomaterials**

The mechanical, biocompatible, hydrogel formation, and degradation properties of biomaterials depend upon the chemical structure of these films. The ability to determine these properties makes the analysis of chemical structure important when characterizing these films. Spectroscopic ellipsometry provides an opportunity to simply determine the thickness of films which could be utilized to determine water uptake and film stability over time. Fourier transform infrared spectroscopy provides an opportunity to determine the extent to which chemical constituencies are retained in the films, as well as an opportunity to determine the amount of cross-linking in these films.

### **2.4.1 Variable Angle Spectroscopic Ellipsometry**

Spectroscopic ellipsometry is the preferred method for film thickness measurement in the semiconductor industry.<sup>38</sup> It is a non-destructive contactless optical technique that allows for the measurement of sample properties based on the changes in polarization of the light that is reflected from the sample.

To characterize a light wave, the wave intensity, frequency, direction of propagation, orientation of vibrations and the variations of all these parameters with time need to be known. The orientational characteristics of the wave in time and space are referred to as the polarization of the wave. “Ordinary” light has no inherent directional quality nor is it affected by phase delays between orthogonal components. However, if all photons of a light beam are oriented in the same direction, the light is referred to as

polarized. This can be achieved by using a source that emits polarized light, laser, or by using a polarizer, a device that allows light of only one particular orientation to pass through. Ellipsometry utilizes two linearly polarized waves with the same frequency but combined out of phase by  $90^\circ$ .

When the beam hits the sample being studied it slows down, changes direction, and is partially absorbed. The sample is characterized by its thickness and by a complex index of refraction:

$$\tilde{N} = n - jk \quad (\text{Eq. 1})$$

Where  $n$  is the index of refraction, the relationship between the speed of light in a vacuum and the speed of light in the material, and  $k$  is the extinction coefficient, the measure of how quickly the light intensity decreases as it passes through the material.

Refractive index and extinction coefficient can be determined by the following:

$$n = \frac{c}{v} \quad (\text{Eq. 4})$$

$$k = \frac{\lambda}{4\pi} \alpha \quad (\text{Eq. 3})$$

Where  $c$  is the speed of light in a vacuum,  $v$  is the speed of light in the sample,  $\lambda$  is the wavelength of the light, and  $\alpha$  is the absorption coefficient.

The value of the refractive index of a thin film as a function of wavelength of the light in the visible region can be described by the Cauchy function:

$$n(\lambda) = A + \frac{B}{\lambda^2} + \frac{C}{\lambda^4} \quad (\text{Eq. 4})$$

Where  $A$ ,  $B$ , and  $C$  are called Cauchy parameters. The extinction coefficient can be described by a similar equation:

$$k(\lambda) = k_0 + \frac{k_1}{\lambda^2} + \frac{k_2}{\lambda^4} \quad (\text{Eq. 5})$$

Where  $k_0$ ,  $k_1$ , and  $k_2$  are called Cauchy extinction coefficients. A second way to model the extinction coefficient is using the Urbach equation:

$$k(\lambda) = \alpha e^{\beta \left( 12400 \left( \frac{1}{\lambda} - \frac{1}{\gamma} \right) \right)} \quad (\text{Eq. 6})$$

Where  $\alpha$  is the extinction coefficient amplitude  $\beta$  is the exponent factor and,  $\gamma$  is the band energy, which is typically set at the lowest wavelength measurable.

### 2.4.2 Fourier Transform Infrared Spectroscopy

Fourier transform infrared spectroscopy (FTIR) is a widely used method for bulk characterization of the chemical composition and chemical bonds in various materials. This technique is based on the absorbance of infrared radiation by chemical bonds at different wavelengths and to different extents.

Electromagnetic radiation is characterized by its wavelength. Radiation with wavelengths between 1mm and  $\sim 1\mu\text{m}$  is referred to as infrared radiation. Wavenumbers, the units most commonly used in IR spectroscopy, refer to the number of waves per unit length, typically a centimeter, and can be calculated by taking the inverse of the wavelength.

The input of energy from the electromagnetic radiation during IR spectroscopy can cause vibrational or rotational excitation in molecules of materials being analyzed depending on the frequency of the light. Molecules can absorb rotational or vibrational energy, thus certain groups can transition from one energy state to another. Every material is permeable to electromagnetic radiation over a wide range, while at certain wavelengths it can be absorbent. So in order for the energy to be absorbed, the frequency

of the incident light must correspond exactly to the energy difference between the two energy states concerned:

$$E_1 - E_2 = h\nu \quad (\text{Eq. 7})$$

Where  $E_1$  and  $E_2$  are the two energy states,  $h$  is the Planck constant, and  $\nu$  is the frequency of the light. The frequency can be related to the wavelength of radiation with the following equation:

$$\nu = \frac{c}{\lambda} \quad (\text{Eq. 8})$$

Where  $c$  is the speed of light and  $\nu$  and  $\lambda$  are the frequency and the wavelength of radiation.

Vibrational excitation of molecules takes place due to the fact that the molecule transitions from lower energy level to a higher one upon absorbing energy, followed by a release of this energy, which causes the molecule to transition back into the lower energy state. When the input energy is lower than what is needed for vibrational excitation of the molecule, rotational excitation occurs.<sup>39</sup>

Fourier transform spectrometers utilize Michelson interferometers to quantify radiation intensity variations due to absorbance by the analyzed material using phase information. The interferometer consists of a beam-splitter that splits the radiation beam emitted by the source into two partial beams, which are then reflected on a fixed mirror and on a movable mirror, and then recombined back onto the beam. Shifting of the movable mirror can cause phase differences between the two partial beams, resulting in a change in interference magnitude. The changes in optical path length are picked up by the detector. For a monochromatic light source a cosine signal is obtained at the detector as a function of the optical path difference  $x$ , also referred to as retardation:

$$I(x) = I_0 \{1 + \cos(2\pi\tilde{\nu}x)\} \quad (\text{Eq. 9})$$

Where  $I$  is the detected beam intensity,  $I_0$  is the partial beam intensity,  $\tilde{\nu}$  is the wavenumber of the light coming from the source, and  $x$  is retardation. For sources with more than one wavelength, the interference pattern is calculated by taking the sum of the cosine signals of all individual frequencies. The interferograms obtained can be converted into a spectrum ( $S$ ) using a Fourier transform:<sup>39</sup>

$$S(\tilde{\nu}) = \int_{-\infty}^{\infty} I(x) \cos(2\pi\tilde{\nu}x) dx \quad (\text{Eq. 10})$$

Wavenumber (cm <sup>-1</sup> )	Assignment	Intensity
3100-3600	-OH stretching	Broad
2972-2952	Methyl C-H antisymmetric stretch	Very strong
2882-2862	Methyl C-H symmetric stretch	Very strong
2960	CH <sub>3</sub> antisymmetric stretch	Medium
2936-2916	Methylene C-H antisymmetric stretch	Very Strong
2863-2843	Methylene C-H symmetric stretch	Very Strong
1750-1725	Methacrylate ester C=O stretching	Strong
1460	CH <sub>3</sub> antisymmetric deformation	Medium
1440	CH <sub>3</sub> symmetric deformation	Medium
1410	Si-CH <sub>3</sub> antisymmetric stretch	Weak
1380-1365	Methyl symmetric bending in Si-CH <sub>3</sub>	Medium to weak
~1270	Si-CH <sub>3</sub> symmetric bending in O <sub>3</sub> SiCH <sub>3</sub>	Strong
~1260	Si-CH <sub>3</sub> symmetric bending in O <sub>2</sub> Si(CH <sub>3</sub> ) <sub>2</sub>	Strong
1210-1160	C-O stretching bands	Multiplets, strong
1200-1000	Si-O-Si stretching	Very strong
~1190	Short-chain Si-O-Si with terminal CH <sub>3</sub> /OH	Very strong
~1135	Short-chain Si-O-Si	Very strong
~1085	Long-chain Si-O-Si with terminal CH <sub>3</sub> /OH	Very strong
~1035	Long-chain Si-O-Si	Very strong
920-830	Si-OH silicon-hydroxyl stretching	Strong
870-750	Si-CH <sub>3</sub> silicon-methyl rocking	Strong
~800	C-Si-C stretching	Strong

**Table 1: FTIR peak assignments for organic and organosiloxane films**

Table 1 provides a list of typical chemical groups found in the films investigated in this project.<sup>38</sup> The table also describes their corresponding peaks found on FTIR spectra, both probable location and intensity.

### 3.0 Experimental

When new drug compounds are developed by pharmaceutical companies, bioavailability tests must be conducted to determine if the drug will be absorbed into the body at a desirable amount. Typically, two different approaches are available for these studies; animal models and cell cultures. Animal studies, in addition to their ethical issues, have additional draw backs. First, these studies can be extremely expensive and time consuming as the test subjects have to be raised to suitable ages before being used. Also, to determine the extent to which the drug is available throughout the body, the subject is euthanized, allowing for single-use only. Finally, it has also been found that animal studies are not always an acceptable representation of how a drug may be absorbed into a human body.<sup>3</sup> Cell cultures are typically carried out using flat porous substrates. Cells are grown to a confluent layer upon the substrate. A compound is then dosed into the apical compartment and measurements are taken over time from the basolateral compartment to determine the transport across the cell layer.<sup>4</sup> These cultures typically use human Caco-2 cells as an *in vitro* model.<sup>5</sup> These cells, though derived from a colon cancer line, are believed to differentiate into a similar phenotype as enterocytes and are a suitable analog to small intestinal epithelium.<sup>6</sup> These studies, however, use flat substrates as well as chemistries which are not seen within the body. It is hypothesized that the lack of cell culture substrate topography and biochemistry are major factors in the difference between *in vivo* and *in vitro* studies. Thus, the overall experimental goal of this project is to more closely mimic the *in vivo* conditions through the incorporation of biomimetic topography as well as biocompatible materials.

This project consists of 5 major proposed experimental objectives. The first step will be to uncover the biological substrate that cells grow on *in vivo* by exposing the basement membrane from a porcine intestine. After the basement membrane has been exposed, a rigid mold will be created via chemical vapor deposition of silica. Once the basement membrane structure has been replicated by a thin silica film, the biological material will need to be removed. Then, a porous mold of the basement membrane will be created via chemical vapor deposition of a biocompatible polymer. The final objective will be to culture intestinal cells upon the polymer mold to determine the cellular response to a more biomimetic substrate.

### **3.1 Introduction of Topography**

While it has been shown that cells respond to topographical cues, most studies of the influence of topography have been restricted to culture substrates with regular, single-scale features, such as grooves. In contrast, *in vivo* topography is highly complex, irregular, and multi-scale. It is hypothesized that introducing topography that more closely mimics *in vivo* topography, cells cultured will exhibit a phenotype more similar to those found in the body.

#### **3.1.1 Small Intestine Preparation and Fixation**

A segment of porcine intestine received from a local abattoir less than 2 hours after slaughter was cut open in the direction of the flow axis, and any bulk material was removed. The tissue was then washed twice with Hanks Balanced Salt Solution (HBSS) and blotted on filter paper to remove mucus. Samples were then placed in a mixture of 1% glutaraldehyde and 1% paraformaldehyde in 0.1M PBS (pH 7.3) at 4 °C overnight. Samples were then cut into small pieces (~1 cm<sup>2</sup>), rinsed in PBS three times, and

subjected to maceration in 0.1% osmium tetroxide ( $\text{OsO}_4$ ) buffer in 0.1M PBS at 20° C for 48 hours. Samples were agitated vigorously to remove all cellular material, rinsed three times in distilled water, dehydrated in a graded ethanol series, and critical point dried.

### **3.1.2 Chemical Vapor Deposition of Silica**

Initial silica depositions were performed in a custom-built stainless steel vacuum chamber approximately 17 L in internal volume. Methylsilane (Gelest 99.9%) was admitted to the reactors through a series of needle valves. Hydrogen peroxide (Sigma Aldrich, 30% by weight) was contained in a Pyrex® jar wrapped in heating tape and volatilized for flow into each reactor through a different set of needle valves. A design of experiments was utilized to find CVD process conditions resulting in silica film deposition, varying flow rate ratio from 1:5 to 1:10, reactor pressure from 1,800 mTorr to 3,000 mTorr and stage temperature from 5 °C to 25 °C.

In an effort to ensure that the monomers were not reacting until they reached the surface, a second custom-built stainless steel vacuum chamber was constructed. This second reactor, approximately 3L in internal volume, has entry ports for each of the two reactants, permitting mixture directly above the stage rather than pre-mixing before the chamber. To find optimal reaction conditions for this configuration, the following process parameter ranges were investigated: total flow rate 9 to 60 sccm, methylsilane to hydrogen peroxide flow rate ratio from 1:5 to 1:10, reactor pressure from 1,000 mTorr to 3,000 mTorr and stage temperature from 5 °C to 25 °C. The concentration of hydrogen peroxide was also varied from 30% to 50% to determine whether a more fully condensed silica network could be formed. Additionally, a gentle annealing (3 hours at 150 °C) was

explored in an attempt to more fully condense the silica network from films that showed evidence of a substantial hydroxyl peak in the FTIR.

In addition to the prepared intestinal samples, silica films were also deposited onto 550 micron-thick silicon wafers from Montco Silicon (lot# S4988) for characterization purposes. All substrates were placed on the deposition stage which was maintained via backside cooling controlled by a Polyscience 6000 series chiller. Vacuum was achieved using an Edwards E2M40 rotary vane pump, and chamber pressure was controlled using a butterfly valve connected to an MKS model 252-A exhaust valve controller and an MKS Baratron capacitance manometer. *In-situ* monitoring of the silica thickness was accomplished using a laser interferometric technique, and the films were grown to a thickness of approximately 1 micron.

### **3.2 Introduce Biocompatible Materials**

Poly(2-hydroxyethyl methacrylate) (pHEMA) has been used extensively in biological and biomedical applications because it is nontoxic and possesses adequate mechanical strength. Applications for pHEMA films include: biosensors, contact lenses, controlled drug release, and resistance to protein adhesion. Chemical vapor deposition provides the opportunity to deposit conformal pHEMA films in a single, solvent-free step.

#### **3.2.1 Photoinitiated Chemical Vapor Deposition of pHEMA**

2-hydroxyethyl methacrylate (HEMA) (Monomer Polymer 98%) and ethylene glycol diacrylate (EGDA) (Monomer Polymer 90%) were used with no further purification or modification. Hydroquinone (Sigma) was added to both liquid monomer HEMA and EGDA to discourage auto-polymerization during heating.

Thin film depositions were performed in a custom-built vacuum chamber, consisting of a quartz viewport at the top to allow ultraviolet light to enter. A low-power ultraviolet lamp (Model UVGL-58, UVP) was placed upon the viewport and emitted light at 254 nm wavelength. The viewport was 1.9 cm thick and the substrate was located 12 cm below the viewport. Thus, the total distance from substrate to the light source was approximately 14 cm. The UV intensity at this distance through the viewport was measured as 50  $\mu\text{W}/\text{cm}^2$  using a UVX radiometer 143 equipped with a UVX-25 sensor.

HEMA and EGDA liquid precursors were vaporized in heated aluminum jars and vapors were admitted to the reactor through separate custom-built shower head devices, such that the flow entered above the stage. HEMA was heated to 75°C, while the EGDA was heated between 40 and 50°C, depending upon the desired flow rate. Vacuum was achieved using a Leybold D8b rotary vane pump, and chamber pressure was controlled using a butterfly valve connected to an MKS model 252-A exhaust valve controller with an MKS Baratron capacitance manometer. Deposition pressure was constant at 75 mTorr. Substrate temperature was maintained via backside contact to the deposition stage, which was cooled by circulation of in house compressed air. Deposition stage temperature was constant at 25°C.

### **3.2.2 Swelling and Degradation Characterization**

A degradation study was performed to determine how the amount of cross-linking would affect the amount of swelling and thickness retention of the deposited films. Films were deposited with different cross-linking (none, low and high) onto pieces of silicon wafer. Each wafer was then broken into 1 inch<sup>2</sup> pieces and then submerged in 2 mL of PBS and incubated at 37°C for varying amounts of time: 24 hrs, 7, 14 and 21 days. Each

degree of cross-linking and each time point were studied in triplicate. Ellipsometry was utilized to determine the thickness of each film before submersion, immediately after coming out of solution, and again after being dried at 60°C overnight. Wet film thickness was used to test the amount of swelling while the dried film thickness was used to determine the amount of degradation. Swelling was calculated in two separate ways: comparing the wet film thickness after 24 hours in soak to the initial film thickness as well as the final film thickness after overnight drying. Degradation was calculated by comparing the final film thickness after overnight drying to the initial film thickness.

### **3.2.3 Biocompatibility Study**

Caco-2 cells were seeded in T-25 flasks at  $7.5 \times 10^4$  cell/mL using Eagle's minimum essential medium (Invitrogen) with 20% fetal bovine serum (American Type Culture Collection, Manassas, VA) and 1% antibiotic-antimycotic solution (10,000 units penicillin, 10 mg streptomycin, and 25  $\mu$ g amphotericin B per mL, Sigma-Aldrich). Cells were maintained at 37°C in a humidified 10% CO<sub>2</sub> incubator in T-25 flasks and split 1:2 after 5 to 7 days when cells reached confluency. Confluent cell layers were treated with 1 mL 0.25% (w/v) Trypsin (Invitrogen) in 0.53 mM EDTA solution and incubated at 37°C for 20 minutes until the cells fully detached. The reaction was stopped by adding 5 mL of media. Cells were then resuspended in cell culture medium at a density of  $2.0 \times 10^4$  cells/mL. A 1 mL suspension was added to each well containing 1cm<sup>2</sup> of test surface material.

Silicon wafers were coated with piCVD deposited pHEMA with different cross-linking densities (none, low, and high). The wafers were then cut into 1 inch<sup>2</sup> pieces and a cuvette was attached to the surface using RTV sealant (100% silicone rubber, Dow

Corning) such that the exposed area of the coated wafer was 1 cm<sup>2</sup>. Polystyrene culture plastic and bare silicon wafer were used as controls. Surfaces were sterilized by treatment with 70% w/v ethanol solution and washing with sterile phosphate buffered saline (PBS).

Cell count and viability determination were conducted 3 days after seeding. The supernatant was decanted and the cells that were attached to the surface were rinsed with 1 mL of PBS and then incubated in 50  $\mu$ L of Trypsin per well at 37°C for 20 minutes until cells were detached from the substrate surface. An aliquot of 200  $\mu$ L of fresh medium was added to each well to stop the reaction. Cell counts were performed using a hemacytometer, where a 1:1 ratio of cells to Trypan Blue (invitrogen) was used to determine cell viability. Percent cell attachment was calculated by dividing the number of attached cells on each surface by the number of cells seeded in each well. Relative cell attachment was calculated by dividing the number of attached cells on each surface by that on polystyrene.

### **3.2.4 Statistical Significance**

In an effort to determine to what extent results differed and were significant, statistical significance analysis was conducted. Statistical significance was tested by applying One-Way ANOVA in the SPSS Statistics 17.0 software suite. A P value less than 0.05 was used to indicate statistical significance.

### **3.3 Characterization Methods to Analyze Biomaterials**

The mechanical, biocompatible, hydrogel formation, and degradation properties of biomaterials depend upon the chemical structure of these films. The ability to determine these properties makes the analysis of chemical structure important when characterizing these films. Spectroscopic ellipsometry provides an opportunity to simply

determine the thickness of films which could be utilized to determine water uptake and film stability over time. Fourier transform infrared spectroscopy provides an opportunity to determine the extent to which chemical constituencies are retained in the films, as well as an opportunity to determine the amount of cross-linking in these films. X-ray photoelectron spectroscopy provides an opportunity to determine the chemical constituencies at the interface of the films. Scanning electron microscopy provides an opportunity to examine the surface features through high resolution micrographs.

### **3.3.1 Spectroscopic Ellipsometry**

Spectroscopic ellipsometry is the preferred method for film thickness measurement in the semiconductor industry.<sup>40</sup> It is a non-destructive contactless optical technique that allows for the measurement of sample properties based on the changes in polarization of the light that is reflected from the sample.

Thin film thicknesses were measured using a J.A. Woollam Co. Inc. M-2000 spectroscopic ellipsometer at angles of 65, 70 and 75°. The Cauchy equation was used to model the system and determine the thicknesses.<sup>41</sup> Thicknesses were collected in triplicate for each sample, and then averaged to obtain an overall thickness for each deposition.

### **3.3.2 Fourier Transform Infrared Spectroscopy**

Fourier transform infrared spectroscopy (FTIR) is a widely used method for bulk characterization of the chemical composition and chemical bonds in various materials. This technique is based on the absorbance of infrared radiation by chemical bonds at different wavelengths and to different extents.

Chemical analysis of the silica thin films was done using a Perkin Elmer Spectrum GX-2000 FTIR running the Spectrum software suite (version 5.3.1). Spectra represent the average of 32 scans over the range between 4000 and 400  $\text{cm}^{-1}$  at a resolution of 4  $\text{cm}^{-1}$ . Measurements were done in absorbance mode, and spectra were baseline corrected using the Spectrum software and thickness normalized for quantitative comparison.

### **3.3.3 X-ray Photoelectron Spectroscopy**

X-ray photoelectron spectroscopy (XPS) is a widely used method for surface characterization of the chemical composition and chemical bonds in various materials. This technique directs a beam of X-rays on a surface while simultaneously measuring the energy and number of electrons that escape from the top 1 to 10 nm of the material.

XPS analysis was performed using a PHI 10-360-4-015 hemispherical analyzer. The instrument is equipped with a PHI 04-173-0-077 Mg/Al dual anode nonmonochromatic X-ray source. Al anode operating at 15 kV and 300 W was used for this analysis. The size of the analyzed spot was 1.1  $\text{mm}^2$ . The base pressure was  $2 \times 10^{-8}$  Torr. Minimum FWHM value was determined by a gold standard, and gold and copper standards were used for energy and scale calibration. A pass energy of 89.45 and 35.75 eV was used for survey and high resolution spectra, respectively. An energy step of 1.0 and 0.05 eV was used for survey and spectra high resolution spectra, respectively. Peak de-convolution and quantification of the elements was accomplished using AugerScan software and Phi sensitivity factors.

Core level	Peak	Origin	Binding energy (eV)	Area (%)
C 1s	1	- C*H <sub>3</sub> - C - C*H <sub>2</sub> - C	285.00	34
	2	- C*(CH <sub>3</sub> ) - CO	285.73	17
	3	- CH <sub>2</sub> - C*H <sub>2</sub> - OH	286.53	17
	4	- O - C*H <sub>2</sub> - CH <sub>2</sub> -	286.89	17
	5	- C*=O	289.10	15
O 1s	1	- C =O*	532.32	33
	2	- O*H	533.09	33
	3	- CO - O* - CH <sub>2</sub> -	533.86	33

**Table 2: High resolution XPS scan data for de-convolution peak fitting.**

Table 2 provides a list of the typical chemical groups found in the investigated films.<sup>42</sup> The table also describes their corresponding binding energies used for de-convolution. XPS peak curve fitting was performed with an 80% Gaussian and 20% Lorentzian peak shape with a Shirley background subtraction.

### 3.3.4 Scanning Electron Microscopy

Scanning electron microscopy (SEM) is a widely used method for obtaining high resolution images of samples surfaces. This technique directs a high-energy electron beam at the sample which interacts with the atoms of the sample producing signals that contain information about the samples surface topography.

Physical feature analysis was conducted using a Hitachi S-4700 FE-SEM. Micrographs were obtained through secondary electron imaging at 3 mm working distance with an accelerating voltage of 2 kV. Aluminum sample holders coated with carbon paint were used as supports for samples. Samples were also sputter coated with gold/palladium using a Cressington Sputter Coater 108 Auto to reduce sample charging.

### **3.3.5 Energy Dispersive X-ray Spectroscopy**

Energy dispersive X-ray spectroscopy (EDS) is an analytical technique used for elemental analysis of a sample. This technique directs a high-energy beam of electrons at a sample to excite and release X-rays from the sample. The number and energy of X-rays emitted from the sample are then collected by the detector. Elemental composition of the sample can be determined because difference in energy between shells and atomic structure are characteristic of specific elements.

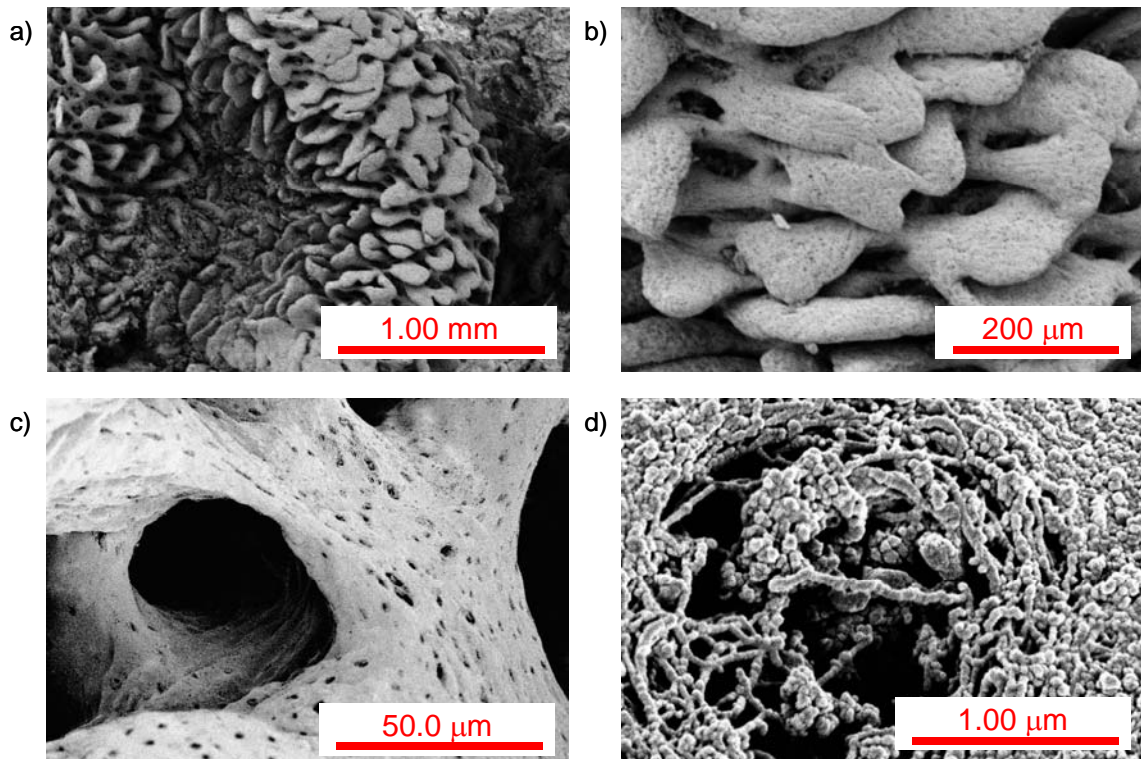
Elemental analysis was conducted using a Phoenix EDAX X-ray analyzer equipped with a Sapphire super ultra thin window detector attached to the Hitachi S-4700 FE-SEM. Samples were analyzed using an accelerating voltage of 20 kV, beam current of 10  $\mu$ A, and a counting time of 100 seconds.

## 4.0 Results and Discussion

It is hypothesized that the lack of cell culture substrate topography and biochemistry are major factors in the difference between *in vivo* and *in vitro* bioavailability studies. Thus, it was imperative to create biomaterials with precise biomimetic micro and nanoscale topographies for use in tissue engineering and drug transport studies. Chemical vapor deposition was utilized in an effort to recreate the irregular, multi-scale topography of the small intestine basement membrane. Also, photoinitiated chemical vapor deposition was utilized in an effort to create biocompatible cross-linked poly(2-hydroxyethyl methacrylate) more chemically similar to conventional spin cast techniques than previously reported plasma enhanced chemical vapor deposited films.

### **4.1 Small Intestine Preparation and Fixation**

To prepare tissue to withstand low pressure in the CVD chamber, dehydration and aldehyde-based fixation techniques were utilized. As we are interested in the topography of the basement membrane that the cells are resting upon, the ultimate goal in tissue processing is to prepare a fixed, dried sample of intact basement membrane with as much of the bulk waste material, cells, and mucus removed as possible. Thus, maceration/osmication with osmium tetroxide ( $\text{OsO}_4$ ) was investigated as a method of removing epithelium and exposing the basement membrane. **Figure 1** shows SEM images of basement membrane that was prepared via this technique.



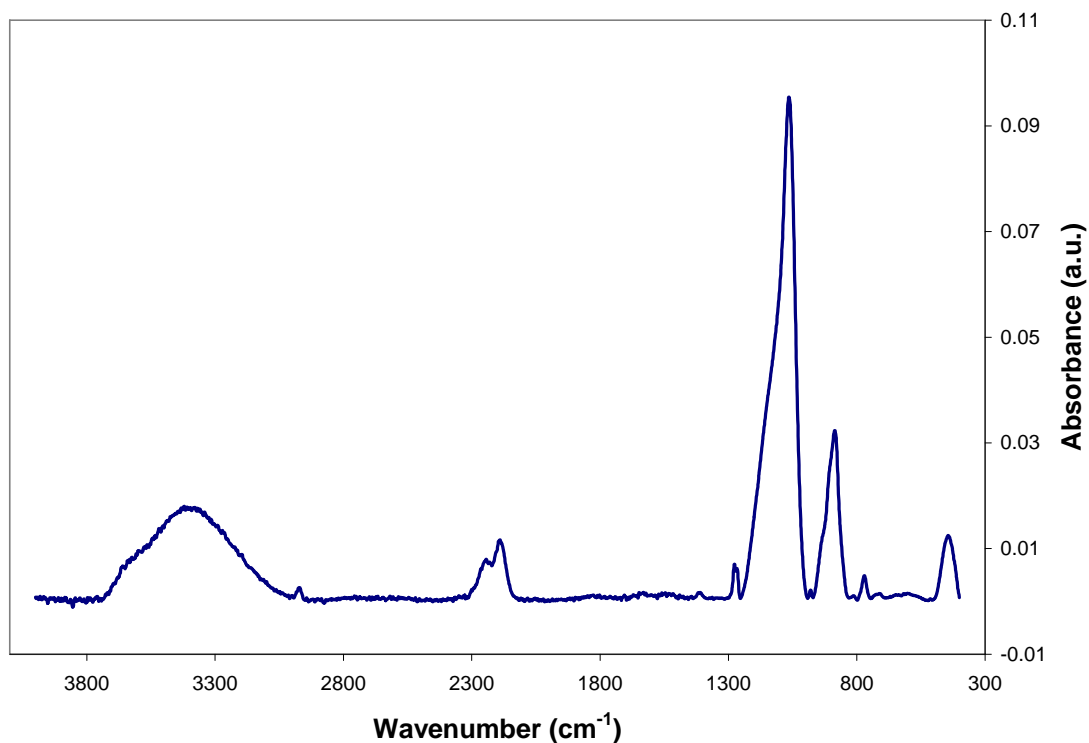
**Figure 1: SEM images of the naked small intestine basement membrane depicting the multi-scale topography intended to be replicated.**

Figure 1a) shows the macroscopic folds, millimeters in scale. On the surface of these folds, finger-like projections called villi and invaginations called crypts, both 100's of micrometers in scale, their proximity can be seen in Figure 1b). Figure 1c) depicts the surface of the intestinal basement membrane, comprised of pores approximately 1-5  $\mu\text{m}$  in diameter. Finally, at the nanometer-scale, fibrous materials in an interwoven pattern provide the ultra-structure of the extracellular matrix, Figure 1d).

#### **4.2 Chemical Vapor Deposition (CVD) of Silica**

In each of two studied CVD reactor configurations, specific operating parameters were established to produce a continuous silica film. In the 17 L reactor configuration, the silica deposition process was sensitive to reactor pressure and stage temperature. All reactions carried out at 1,800 mTorr led to no deposition, possibly due to a low residence

time associated with a low pressure in a large volume, thus not allowing the reactants to reach the stage and react. However, it was found that at a methylsilane to hydrogen peroxide flow rate ratio of 1:5, 3,000 mTorr reactor pressure and 25 °C stage temperature, a reaction occurred that produced a powder rather than a thin film. The formation of a powder suggests that the reaction is taking place above the stage, rather than on the surface. Final reaction conditions for this reactor configuration utilized a methylsilane to hydrogen peroxide flow rate ratio of 1:5 (total flow rate 60 sccm, total residence time 280 min), 3,000 mTorr reactor pressure and 5 °C stage temperature produced a silica film, as confirmed by FTIR (**Figure 2**), at a deposition rate of 10 nm/min.



**Figure 2: FTIR spectra of a silica film deposited on silicon wafer.**

Spectroscopically, the sample shows a large Si-O absorption in the characteristic location between 1000 and 1200 cm<sup>-1</sup>, which is indicative of the silica network. Also

prominent is a larger –OH absorption in the high wavenumber region, most likely due to Si-OH bonds created during the deposition step that were not condensed to produce Si-O-Si bonds. This is supported by the presence of the large absorption between 830 and 920  $\text{cm}^{-1}$  that corresponds to Si-OH bonding. A small amount of organic C-H bonding is evident at approximately 2800  $\text{cm}^{-1}$ , due to retention of the  $\text{CH}_3$  group in the silane monomer. Also present is Si-H bonding, appearing at 2200  $\text{cm}^{-1}$ . The presence of the Si-H bonds, coupled with the large –OH peak, suggests that this silica network is not fully condensed, as we would expect no Si-H bonding and minimal -OH incorporation in the final coating if all Si-H sites were reacted.

In the second reactor configuration, the identical optimal reaction conditions from the first reactor were initially examined, but it was found that these conditions caused the hydrogen peroxide, the only liquid precursor, to condense on the surface, rather than create a silica thin film. This initial problem was solved by raising the stage temperature to 25 °C to avoid liquid formation on the stage. However, at these reaction conditions (total flow rate 60 sccm, flow rate ratio of 1:5, 3,000 mTorr, 25 °C), films were non-uniform (i.e. standard deviation of 119nm with total mean thickness 422 nm when three thickness readings were taken on a 1 inch square piece of wafer). Flow rates were then adjusted to allow a residence time similar to the first reactor (methylsilane flow rate of 3 sccm, total flow rate 26 sccm), accounting for the significant decrease in reactor volume; these reaction conditions resulted in cloudy films, possibly due to incorporation of hydrogen peroxide and formation of a hydrogel-type film. In fact, a full factorial design of experiments, exploring high (3,000 mTorr) and low (1,500-1,800 mTorr) reactor pressures, as well as methylsilane to hydrogen peroxide ratios of 1:5, 1:7.5, and 1:10

revealed that all reactions at high (3,000 mTorr) pressure or a reactant ratio of 1:10 resulted in cloudy films. These results demonstrate the sensitivity of the CVD silica process to operating parameters, including stage temperature, flow rates of reactants, and reactor pressure. Final reaction conditions for this reactor configuration utilized methylsilane to hydrogen peroxide flow rate ratios of 1:5-1:7.5 (total flow rate 26 sccm, total residence time 120 min), 1,500-1,800 mTorr reactor pressure and 25 °C stage temperature, a reaction occurred that produced a uniform silica thin film, as determined by ellipsometry, at a deposition rate of approximately 20 nm/min.

#### **4.2.1 Small Intestine Replication via CVD Silica**

Once reactor conditions producing silica thin films were established in each reactor configuration, intestinal samples were coated with silica in the vacuum chamber. Blank pieces of silicon wafer were placed next to the fixed, dehydrated intestinal samples to provide visual feedback and confirmation of silica growth during the deposition. Examination of topographical features of uncoated and coated intestinal basement membrane at the macro- and micro-scale demonstrates the capabilities of CVD to replicate biological features at multiple scales (**Figure 3**).

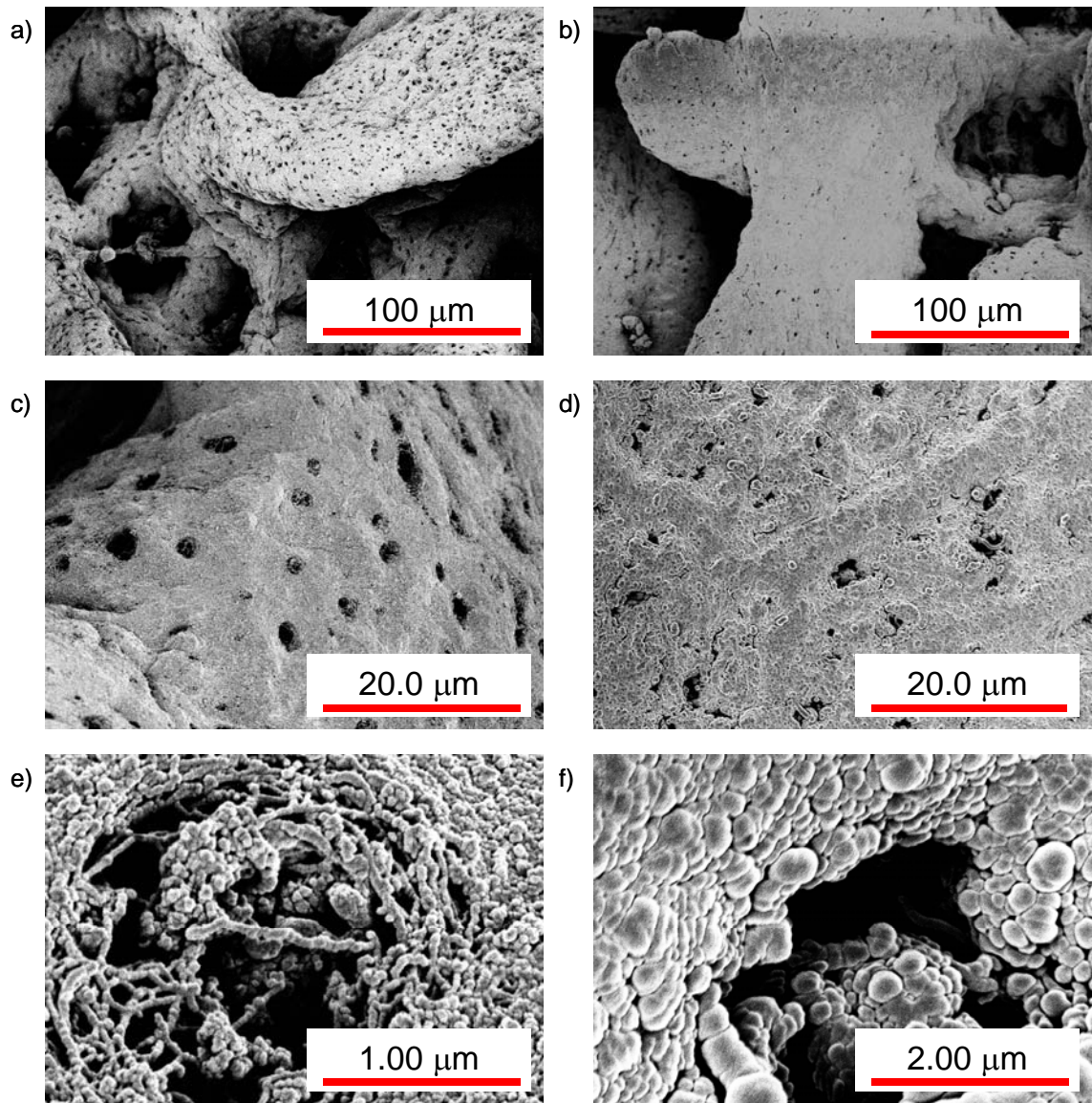


**Figure 3: SEM images of uncoated (a, c, e) and silica coated (b, d, f) porcine intestine basement membrane.**

The macroscopic folds of intestinal tissue as well as the microscopic crypt-villus topography were clearly conserved during coating with silica (Figure 3a-b). The pores in the intestinal basement membrane (Figure 3c-d), which are on the order of 2 μm in diameter, were also successfully replicated. However, examination of the topography at the sub-micron scale reveals fibrous material that is masked by spherical structures

(Figure 3e-f). These spherical structures appear to result specifically from CVD on biological material as silica depositions on silicon wafers resulted in a flat nano-scale surface observed by SEM. Confirmation of the presence of the silica coating on the biological substrate is provided via EDS analysis (**Figure 4**).

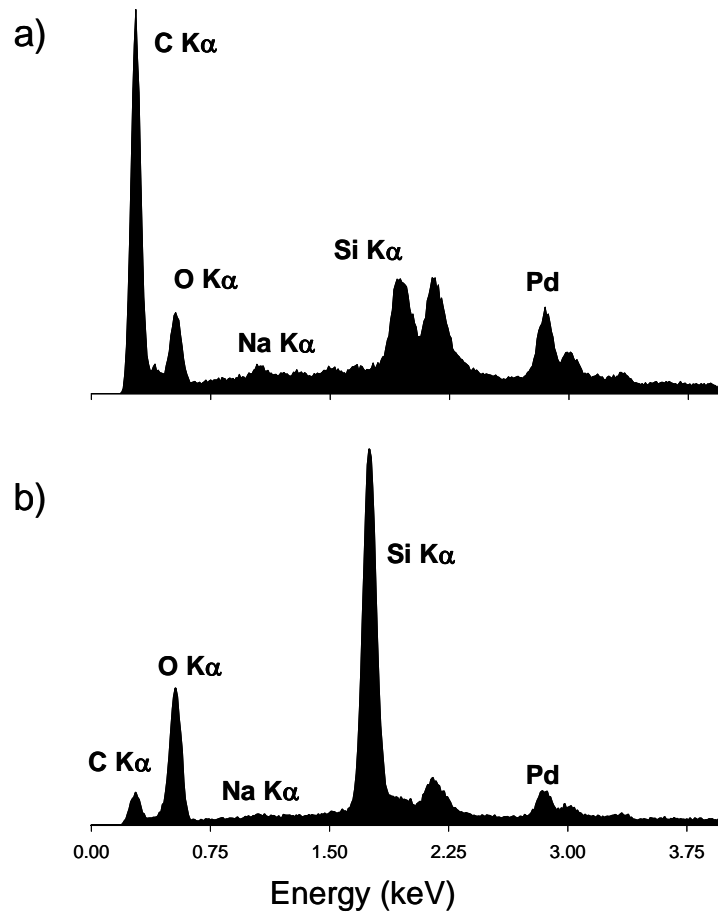


**Figure 4: EDS spectrum of the a) uncoated and b) silica coated intestinal basement membrane. Note that the large Si peak that appears on the sample that has undergone the silica deposition step, as opposed to the C-dominated spectrum for the native tissue.**

As can be seen, the EDS spectrum of the uncoated intestinal sample is dominated by the carbon peak, indicative of the organic nature of the intestinal sample (Figure 4a), whereas the coated sample (Figure 4b) shows a large increase in the Si and O peaks,

indicative of the silica network on the sample surface. Further examination shows that the C peak still has a small presence in EDS spectra. It is believed that this can be attributed to the sampling depth of the electron beam, approximately 1  $\mu\text{m}$ , being very similar to the thickness of the silica film deposited, approximately 1  $\mu\text{m}$ . Also there is some residual carbon in the silica network, since we used an organosilane and not a pure silane.

#### **4.2.2 CVD Process Parameter Variation**

Additional experiments were conducted in an attempt to fully condense the silica network and improve the integrity of the stand-alone replica. It is hypothesized that a film with more long-chain silica will have greater mechanical stability as well as a more uniform surface topography at the nano-scale. Higher concentrations of hydrogen peroxide were investigated to more fully react the Si-H groups in the methylsilane precursor. FTIR analysis indicated that the hydroxyl content within the films remained approximately constant (area under the hydroxyl peak relative to the entire scan decreased from 28% to 26%), when hydrogen peroxide concentration increased from 30% to 50%. Further optimization of the silica reaction included exploring films produced by varying reactor pressure from 1,500 to 1,000 mTorr, reactant ratio from 1:7.5 to 1:5, and methylsilane flow rate from 3 to 1.5 sccm. It was believed that by lowering the reactor pressure, the reactants would be able to reach the substrate surface with less chance of reaction in the vapor phase. Also, by lowering the reactant flow rates into the reactor, it was believed that reduction in potential turbulence might also promote reaction on the surface rather than in the vapor phase. Furthermore, by varying the

reactant ratio, it was hypothesized that we would create a more fully condensed, long-chain silica network with fewer pendant hydroxyl groups.

Lowering the overall reactor pressure or changing the reactant ratio to one which was closer to the stoichiometric ratio of silica (1:4), did not have a dramatic affect on the chemistry of the silica films, observed through FTIR analysis. This result was somewhat unexpected, as it was believed that having fewer hydroxyl radicals present in the reactor due to the lower reactant ratio (1:5) would promote long-chain formation while decreasing the likelihood of creating hydroxyl-saturated silicon molecules. Slower flow rates, however, did notably decrease the hydroxyl peak and increase long-chain silica formation observed via FTIR, most notably at a total reactor pressure of 1,500 mTorr and reactant ratio of 1:5 (**Figure 5**).

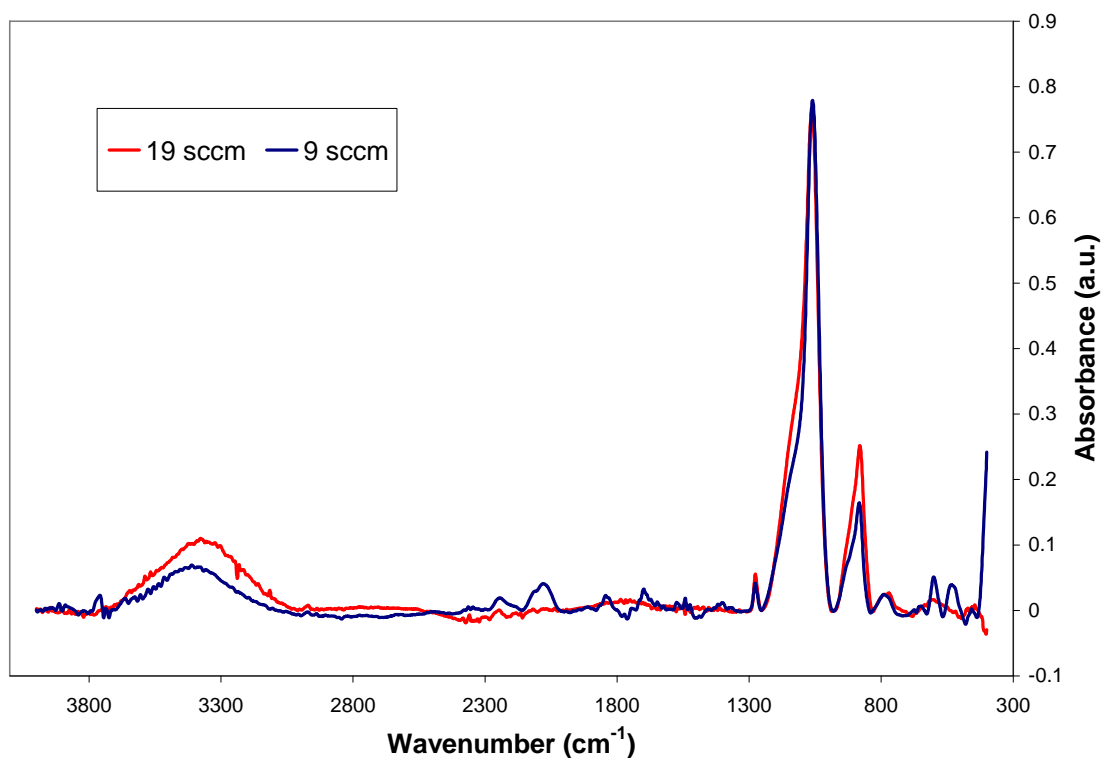


**Figure 5: FTIR spectra of the final silica deposition optimization showing the positive effect of lowering overall flow rate into the reactor.**

SEM analysis confirmed that these process parameter changes did not, however, translate to a change in the sphere formation during deposition on intestinal tissue, and there also was not a notable improvement in the mechanical integrity of the film.

Finally, a gentle post-deposition anneal was examined to determine whether it was possible to drive Si-OH condensation. FTIR analysis (**Figure 6**), confirmed that the hydroxyl peak was significantly decreased from about 52% to 20% following a 3 hour anneal at 150 °C.

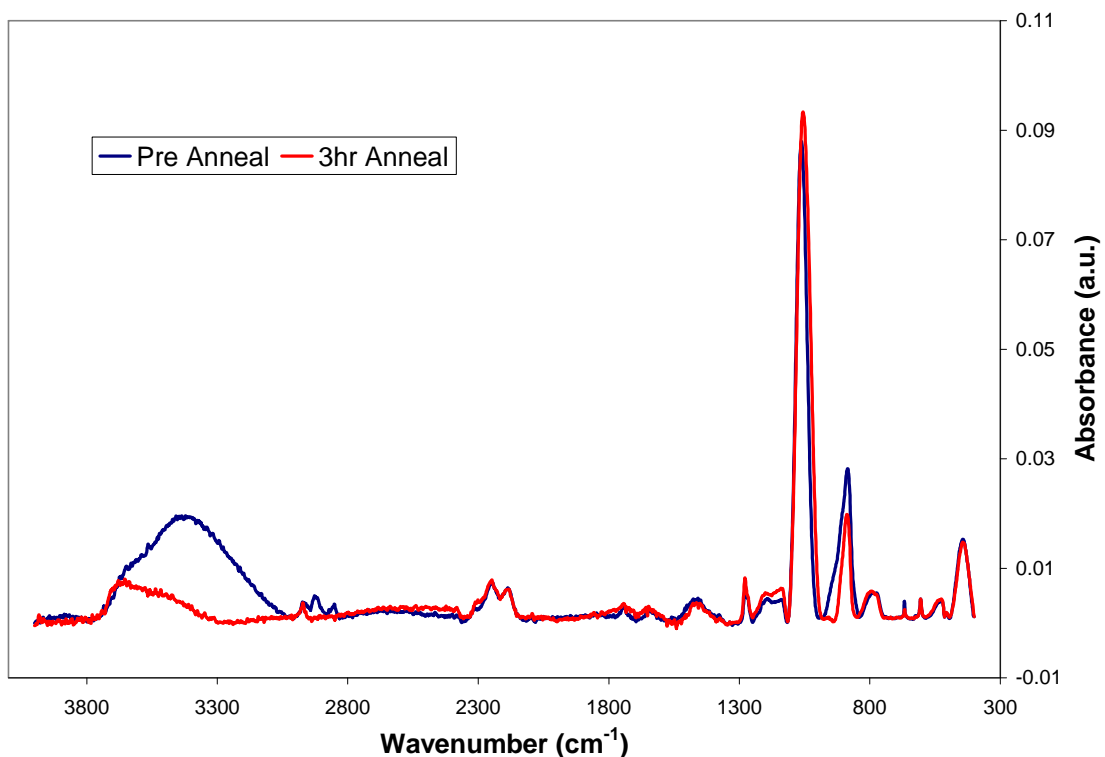


**Figure 6: FTIR spectra showing the dramatic lowering of hydroxyl in the silica film after a gentle post deposition annealing process.**

### **4.3 Photoinitiated Chemical Vapor Deposition (piCVD) of Biomaterial**

Photoinitiated chemical vapor deposition (piCVD) utilizes an ultraviolet light source to selectively decompose a chemical initiator to form free radicals. The UV light

provides photons at specific wavelengths which are known to radicalize specific chemical bonds. However, because piCVD does not involve plasma or high temperatures, it is a useful method for depositing films on sensitive materials.

#### 4.3.1 piCVD of Non Cross-linked pHEMA

As in previously described piCVD processes, HEMA is the only species introduced into the reactor.<sup>37</sup> There is no separate photoinitiator required, so it is concluded that polymerization is initiated by UV irradiation of the HEMA monomer itself. FTIR analysis reveals that the piCVD pHEMA film contains the major chemical constituents of the HEMA monomer itself (**Figure 7**).

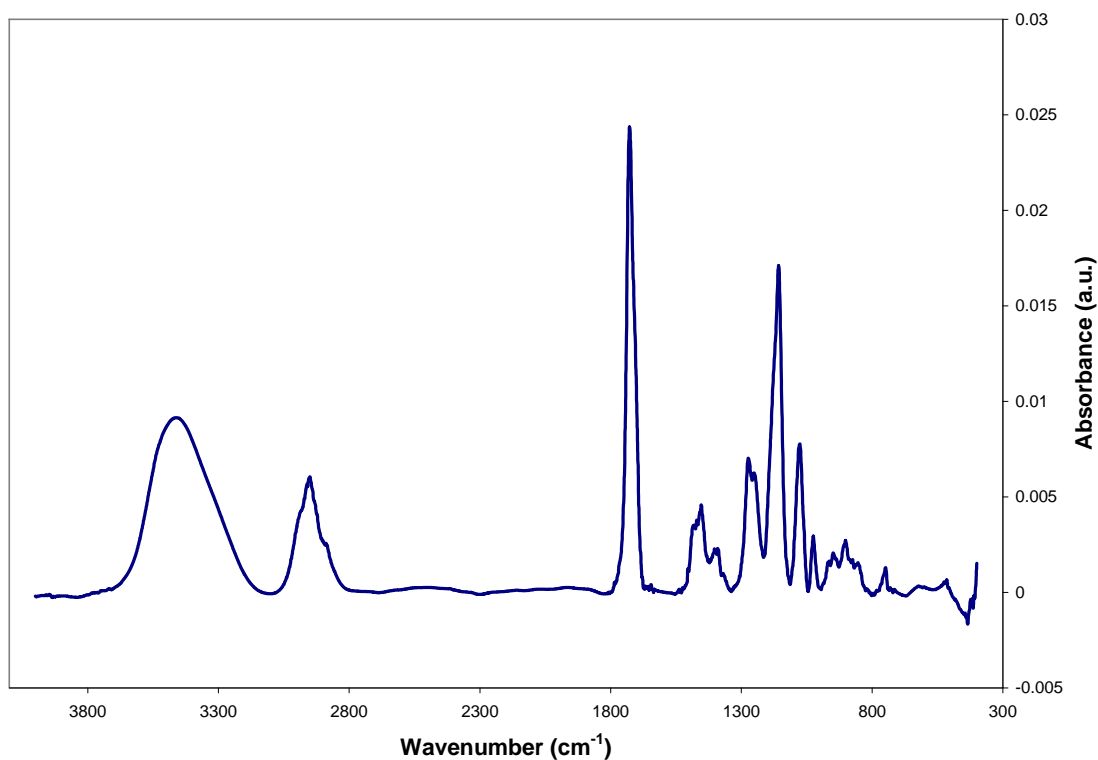


**Figure 7: FTIR spectra of non cross-linked pHEMA illustrating the retention of chemical constituencies from the liquid monomer.**

The regions to consider are the broad peak between 3100 - 3600  $\text{cm}^{-1}$ , attributed to the hydroxyl group; the two peaks between 2800 - 3000  $\text{cm}^{-1}$ , attributed to the symmetric and antisymmetric stretch of methyl groups; a strong peak between 1725 - 1750  $\text{cm}^{-1}$ , attributed to the carbonyl group; and the triplets between 1050 - 1300  $\text{cm}^{-1}$ , attributed to the ester.<sup>38</sup> The overall retention of the monomer functional groups demonstrates that the radicalization does not have a detrimental effect on the HEMA backbone.

XPS was utilized to further characterize the atomic makeup of the piCVD pHEMA films. It was expected that there would be multiple bonding states within the oxygen 1s peak corresponding to the three different bonding configurations in the films; carbonyl ( $\text{C}=\text{O}^*$ ), hydroxyl ( $\text{O}^* - \text{H}$ ), and ester ( $\text{CO} - \text{O}^* - \text{CH}_2$ ). The carbonyl peak was set as the reference (533.6 eV) and peak separations of 0.79 and 1.48 eV were used for the hydroxyl and ester peaks, respectively. The de-convoluted peaks for these three moieties have total peak area ratios of 1 : 0.89 : 0.91 with respect to carbonyl (**Figure 8**).

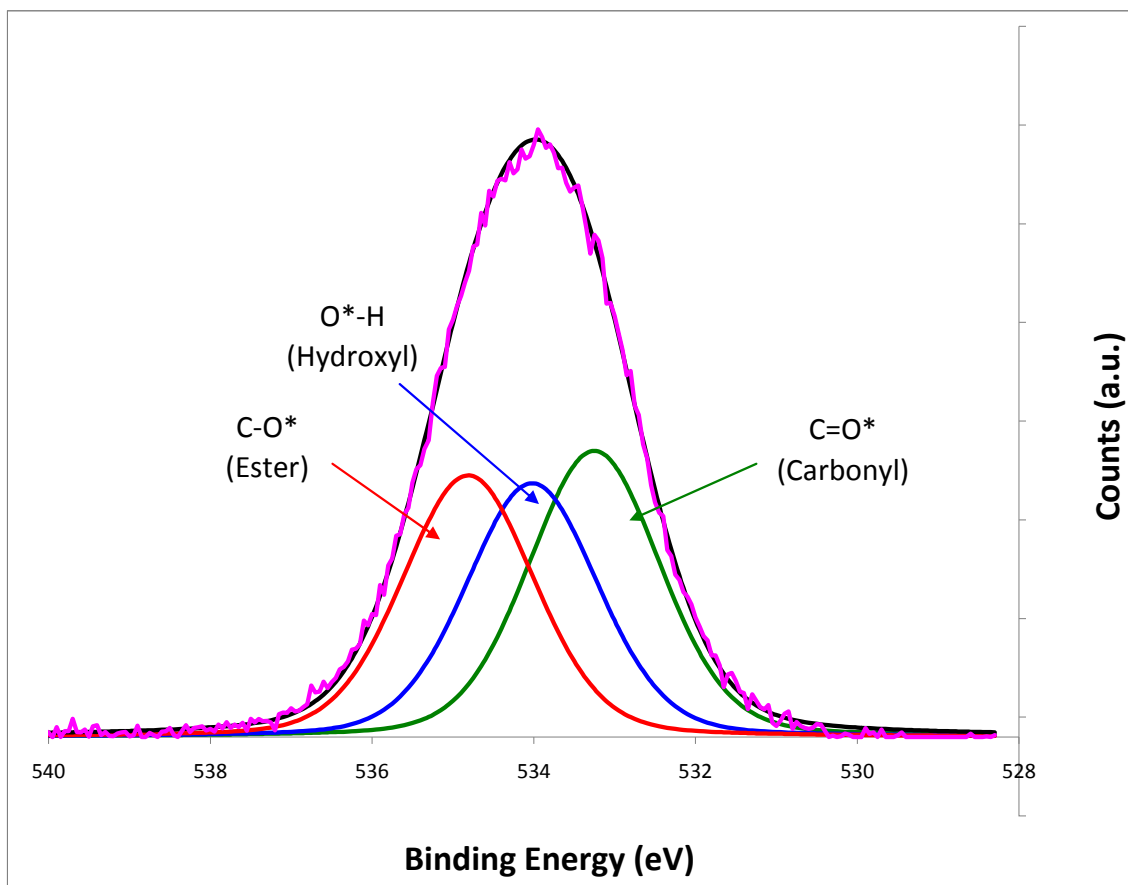


**Figure 8: XPS oxygen 1s atomic spectra with de-convoluted peaks for non cross-linked pHEMA films.**

These ratios compare favorably to the inherent make-up of a HEMA molecule, with ratios of 1 : 1 : 1. However, there are possibly multiple activation pathways during radicalization that would account for the change in relative amounts of the oxygen functional groups. For example, UV wavelengths below 267 nm have been demonstrated to cause initiation of the carbonyl species.<sup>43</sup> The fact that the films deposited here have overall retention of the carbonyl with respect to the other two oxygen-containing moieties supports the proposed mechanism of vinyl bond radicalization<sup>37</sup> for initiation and propagation of polymerization.

### 4.3.2 Cross-linking of pHEMA with Ethylene Glycol Diacrylate (EGDA)

It was desired to tailor the chemical properties of the films by introducing a cross-linker. EGDA was chosen due to the similarities of functional groups compared to HEMA, supporting potential ability to be initiated by UV irradiation. Because EGDA contains no hydroxyl group, it should be possible to use it to tune the hydrophobicity of the films to the desired level.

As a higher flow rate of EGDA is introduced to the reactor, the relative amounts of functional groups within the films changes (**Figure 9**), indicating incorporation of EGDA cross-linker.

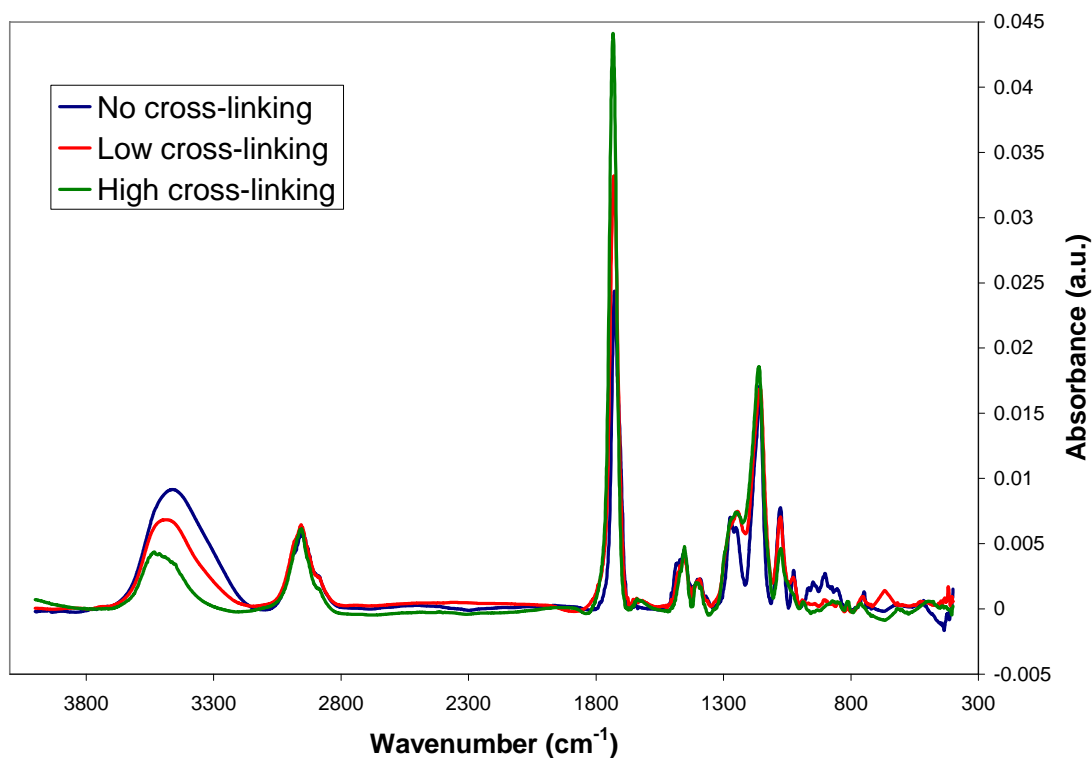


**Figure 9: FTIR spectra exhibiting the incorporation of chemical cross-linker. The inverse variation of hydroxyl and carbonyl peak intensity is due to EGDA having no –OH and two C=O groups.**

As expected, the addition of EGDA, with its two carbonyl groups, causes an increase in the peak between 1725 - 1750  $\text{cm}^{-1}$ . Also, because EGDA contains no hydroxyl group, a decrease in the peak between 3100 - 3600  $\text{cm}^{-1}$  was expected. However, it is important to note that the hydroxyl peak has not been completely removed, showing the HEMA monomer has not been completely saturated with cross-linker.

XPS analysis was utilized to characterize the degree of cross-linking in the films.

**Figure 10** shows the de-convoluted oxygen 1s peak for the three different films.

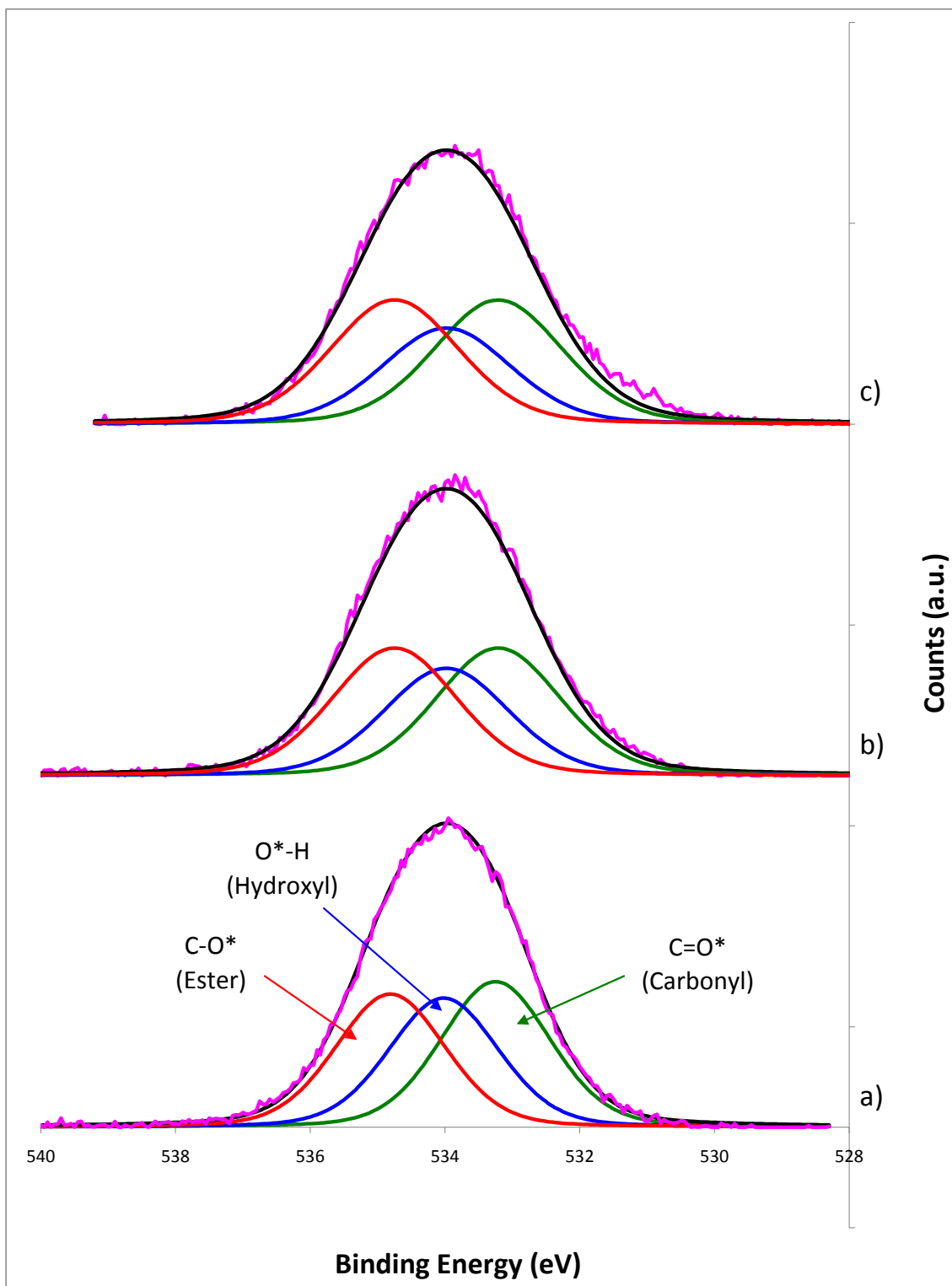


**Figure 10: XPS oxygen 1s atomic spectra with de-convoluted peaks for a) non, b) low, and c) high cross-linked pHEMA films. The relative loss of hydroxyl area under the de-convoluted peak confirms the incorporation of EGDA.**

The area ratios of carbonyl/hydroxyl/ester are 1 : 0.83 : 1 and 1 : 0.78 : 1 for the low and high cross-linked films, respectively. These results are expected and support FTIR analysis: as more EGDA, containing two carbonyl groups and no hydroxyl, is incorporated into the films, there is a decrease in the relative amount of hydroxyl found in the films. It was also expected that the ratio of carbonyl to ester would be close to 1:1, as these two groups are found in this ratio in both HEMA and EGDA. These results are also confirmed by carbon 1s deconvolution (data not shown). The percentage of cross-linking can also be estimated from previous XPS relationships relating the peak intensities of moieties attributed to EGDA and HEMA<sup>36</sup> at approximately 10% and 15% for the low and high cross-linked films, respectively. It is also interesting to note that there is approximately 6% cross-linking found in the homopolymer film, possibly due to the multiple radicalization pathways. Examination of the full width at half maximum for the three de-convoluted peaks showed a change from 1.92 eV for non cross-linked to 2.26 eV for the high cross-linked film, suggesting multiple radicalization pathways and a more complex bonding environment.

#### **4.3.3 Hydrogel Formation and Degradation of Non, Low, and High Cross-linked pHEMA**

Water uptake and degradation of the piCVD pHEMA films were investigated as their intended use is as a cell culture substrate. The hydration study tested how much the film would swell during exposure to solution over a 24 hour period, and to what extent the cross-linking of the films would affect the degree of water uptake. The degradation study was used to determine what thickness loss may occur in deposited films over a

typical cell culture time period of 21 days, and to what extent the cross-linking would affect film stability.

#### ***4.3.3.1 Film Swelling***

Film swelling was calculated by comparing the wet film thickness after 24 hours in soak to the initial deposited film thickness. Some films lost thickness after 24 hours and thus exhibit a negative swelling percentage in comparison to the original deposited film thickness. It was seen that the non cross-linked films exhibited a -36% swelling while the low and high cross-linked films swelled 1.3% and 1.8%, respectively. To determine a more representative degree to which films swelled, the wet film thickness after 24 hours in soak was then compared to the final film thickness after over night drying. **Figure 11** shows the amount of film swelling as a percentage of the final thickness.

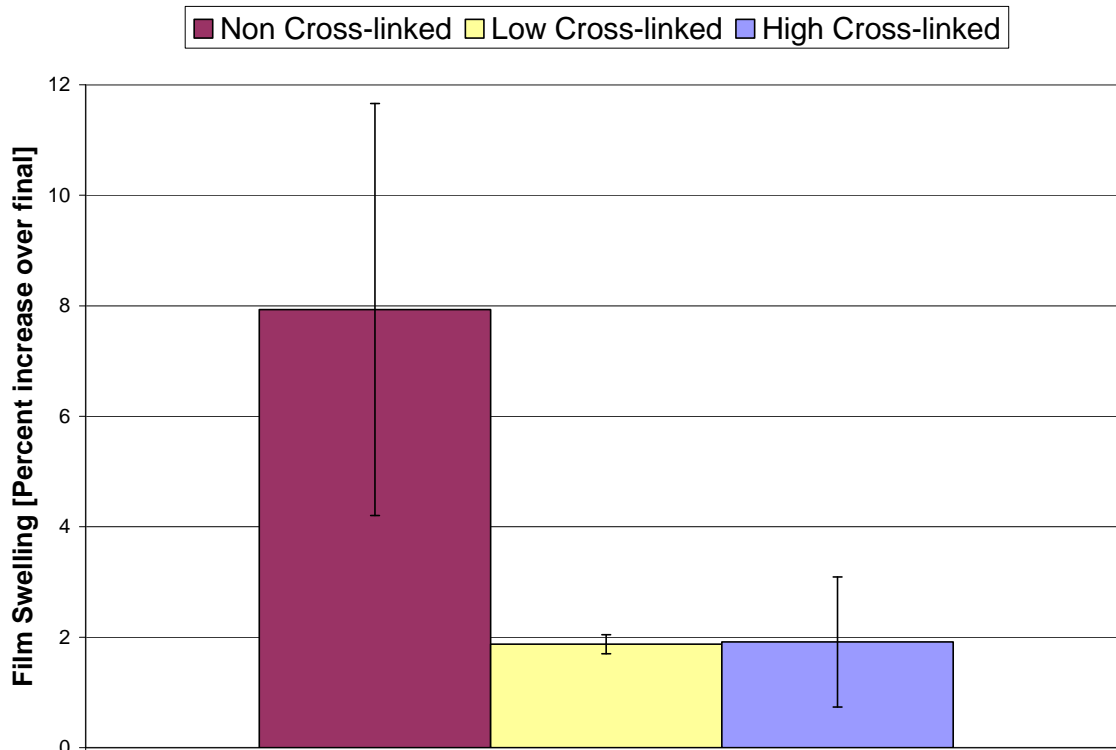


**Figure 11: Film thickness increase as a function of cross-linking after 24 hours in solution. High error in non cross-linked films is due to 40% overall thickness loss after 24 hours.**

Some films lost thickness after 24 hours and thus exhibit a negative swelling percentage in comparison to the original deposited film thickness. The highest amount of swelling (8%) was, as expected, in the non cross-linked films, as those were the most hydrophilic. There was no statistically significant difference in swelling between the two cross-linked films, which each swelled approximately 2%. The incorporation of a hydrophobic cross-linker in addition to the inherent cross-linking of the piCVD films decreased the ability of the films to take up water and swell. Large error may be attributed to the overall thickness loss of the non cross-linked films, as described below. These results are similar to those observed with PECVD films, for which non cross-

linked films had the greatest amount of swelling (12%), and low and high cross-linked PECVD films swelled 3% and 1%, respectively.

#### 4.3.3.2 Film Degradation

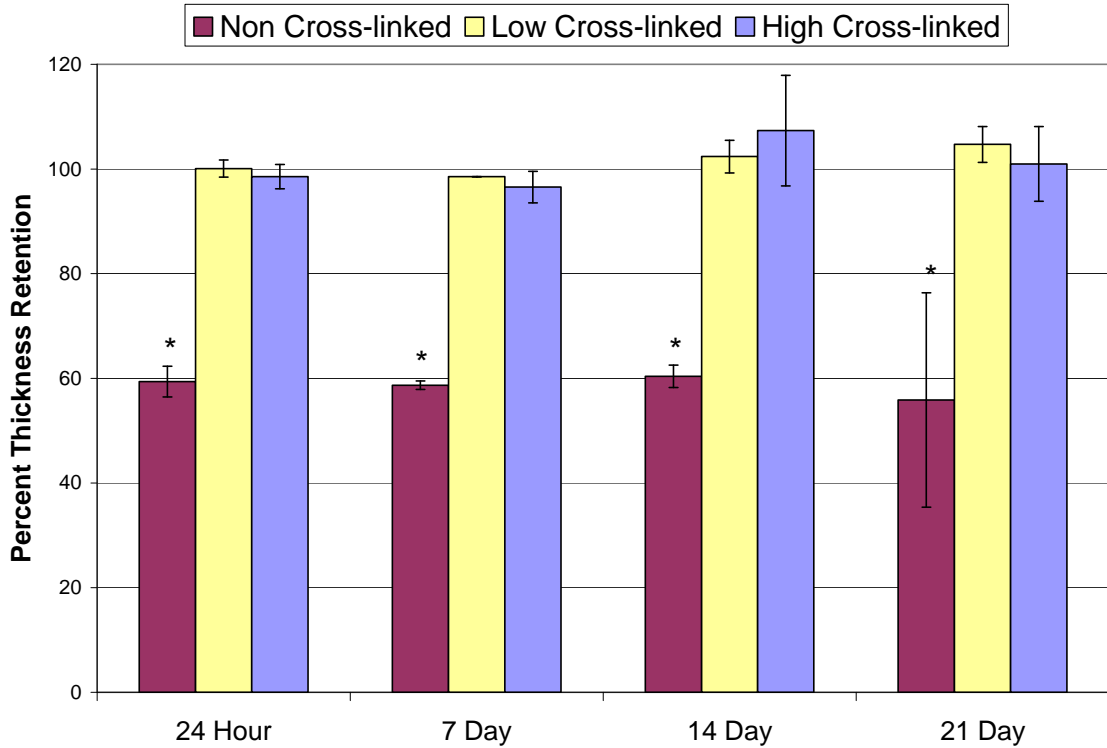


**Figure 12: Degradation profiles as a function of cross-linking over a 21 day time period. Non cross-linked films retained integrity after an initial thickness loss. Cross-linked films retain thickness throughout the duration of the study. (\*) indicates statistical significance compared to cross-linked films ( $p < 0.0005$ )**

**Figure 12** shows the amount of thickness loss as a percentage of the original deposited thickness after incubation in buffer for varying periods of time. It is interesting to note that the non cross-linked films exhibited a roughly 40% loss in thickness after just 24 hours. However, these films maintained approximately 60% of their thickness up to 21 days. It is thought that the inherent cross-linking caused by UV irradiation may have strengthened the film such that after an initial erosion of loosely bound material, the films

were stable for the remainder of the test period. Similar to the swelling observations, there appears to be no statistically significant difference between the two cross-linked films, both maintaining nearly 100% of their original thickness after 21 days incubation. Apparent increases in thickness may be attributed to ellipsometry readings taken on portions of the films that, when dried, may have not been lying flat. The degradation behavior of piCVD pHEMA differs considerably from that of PECVD films, which degraded continuously throughout 21 days in aqueous conditions, with a total thickness loss over this time period of 27% and 12% for low and high cross-linked films, respectively. Non cross-linked pHEMA was not included in this study due to rapid and complete degradation within 7 days in solution.

#### **4.3.4 Cell Attachment Study**

A three day cell attachment study was conducted to assess biocompatibility of the deposited films. Percent cell attachment was determined by comparing the number of cells attached to each surface to the number of cells seeded in each well. It was seen that cells attachment was 575% for polystyrene, 290% for non cross-linked, and 533% and 633% for low and high cross-linked films, respectively. Relative cell attachment was determined by comparing the number of cells attached to polystyrene, a traditional cell culture material, to the prepared non, low and high cross-linked pHEMA films, as well as bare silicon wafer as a control.

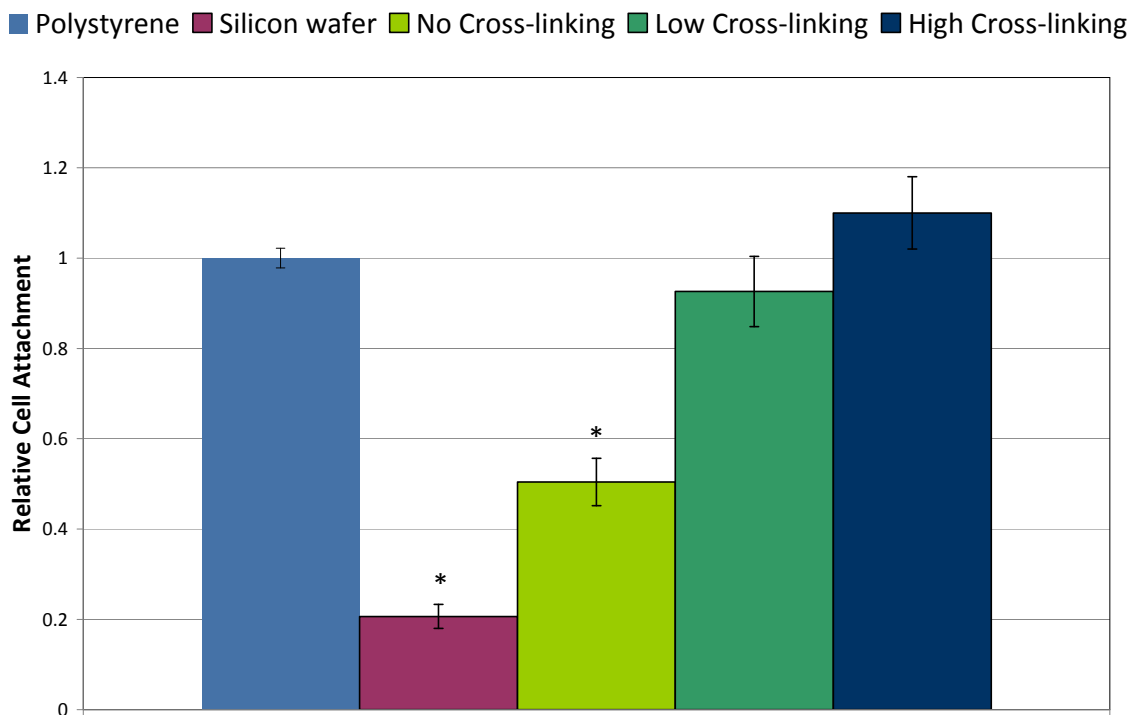


**Figure 13: Relative cell attachment on thin films compared to polystyrene after 3 day cell culture. Cross-linking shows improved cell attachment when compared to non cross-linked films. (\*) indicates statistical significance compared to polystyrene and the cross-linked films ( $p < 0.05$ )**

**Figure 13** shows that after 3 days, the low and high cross-linked films compared favorably to polystyrene, at approximately 93% and 110% attachment, respectively. In contrast, non cross-linked films showed approximately 50% attachment. It is also important to note the significant increase in relative cell attachment from that on silicon wafer (20%), the base material on which the pHEMA films were deposited. Similar cell viabilities were achieved on the different surfaces: polystyrene (88%), non cross-linked pHEMA (81%), low cross-linked pHEMA (86%) and high cross-linked pHEMA (87%). The high relative cell attachment and viability of cells illustrate the suitability of cross-linked piCVD pHEMA films as a culture substrate. Interestingly, relative cell attachment

on piCVD pHEMA was greater than that on PECVD pHEMA, which was 36% and 67% for low and high cross-linked films (85% viability), respectively. Non cross-linked pHEMA was not included in these studies due to rapid film degradation.

## 5.0 Conclusions

A single-step chemical vapor deposition (CVD) process at moderate temperature and pressure has been used to deposit conformal silica films on fixed and dehydrated biological material. The irregular, multi-scale complex topographical features of intestinal basement membrane have been replicated to the micro-scale in silica. The porous structure of intestinal basement membrane, representing features on the order of 1-5  $\mu\text{m}$  in scale, was replicated, but fibrous structures below 1  $\mu\text{m}$  in scale were masked. Further process variation produced changes in chemical structure as exhibited by FTIR spectra. However, these changes did not lead to the desired reduction of sphere-like formations on the surface of substrates. It was also seen that a gentle, post deposition annealing step drastically reduced the hydroxyl content within the silica films. Creation of this reusable non-biological mold is the first step in deposition of biocompatible polymer membranes with precisely biomimetic topography, which could be highly useful in cell culture and tissue engineering applications.

This work also demonstrates the ability to cross-link pHEMA films using photoinitiated CVD, simply by adjusting the ratio of HEMA to EGDA flowed into the CVD reactor. Also, tuning the cross-linking of these films allows for controllability of swelling and degradation properties. Cross-linked films had greater stability, demonstrated by minimal swelling and degradation, when compared to non cross-linked pHEMA films. Cross-linking also affected the degree to which cells attached to the polymer substrates, such that cross-linked films met the industry standards of polystyrene. Taken together, these results support the suitability of piCVD for coating of

cell culture substrates or for use as a scaffold material with tunable swelling and degradation properties.

## 6.0 Recommendations

Silica films deposited via chemical vapor deposition (CVD) have the ability to recreate biological structures as small as 150 nm. However, it was found that silica films were comprised of sphere-like nanostructures that masked the fibrous makeup of the intestinal basement membrane. Further experiments were conducted in an effort to reduce hydroxyl content within the films, and create a silica network consisting of more long-chain silica. Although the experiments were able to remove some of the hydroxyl content, the sphere-like structures were not eliminated from the surface. In addition, it was found that in an effort to decrease the hydroxyl content, the deposition rate of the silica films was 4 nm/min. This deposition rate would require depositions of over 4 hours to create a micron thick layer upon the intestine. For these reasons, it may be recommended that silica CVD may not be the best option for replicating the structure of the small intestine.

Annealing of the silica films showed a dramatic decrease in the hydroxyl region. However, annealing was not conducted on films deposited on the biological substrate. Further work may include annealing silica films while they are still on the biological substrate to remove hydroxyl content and create a more condensed silica network. However, this would add an additional step to the process, further complicating the problem.

Photoinitiated CVD (piCVD) produced pHEMA films of high chemical purity. Recommended work would include depositing pHEMA films of varying cross-linking via initiated CVD and characterizing their biocompatibility, which

has not been done to date. Also, redepositing pHEMA films via plasma enhanced CVD with lower power plasma might create more chemically pure pHEMA films, affecting the biocompatible and biodegradable properties of these films. It was also seen that the piCVD films exhibited delamination during incubation. Further work would include varying the substrate temperature in an effort to ensure that films were attached to the surface. Also, future work could utilize this delamination to its advantage, by depositing a thin pHEMA film on a substrate with topography and determining if a simple soak could remove the film.

## 7.0 References

- 1 *Oral Drug Delivery Market – Controlled and Sustained Release to be Major Revenue Generators*. GBI Research, 2010.
- 2 Bockus, H. L. *Gastroenterology*, Saunders, Philadelphia, Vol. 2, 1974.
- 3 Perel, P., I. Roberts, E. Sena, P. Wheble, C. Briscoe, P. Sandercock, M. Macleod, L. E. Mignini, P. Jayaram, K. S. Khan, *Comparison of Treatment Effects Between Animal Experiments and Clinical Trials: Systematic Review*. *BMJ*, 334 (7586), 2007.
- 4 Ranaldi, G., K. Islam, Y. Sambuy, *Epithelial Cells in Culture as a Model for the Intestinal Transport of Antimicrobial Agents*. *Antimicrob Agents Chemother*, 36 (7), 1374-1381, 1992.
- 5 Wilson, G., *Cell Culture Techniques for the Study of Drug Transport*. *Eur J Drug Metab Pharmacokinet*, 15 (2), 159-163, 1990.
- 6 Hidalgo, I. J., T. J. Raub, R. T. Borchardt, *Characterization of the Human Colon Carcinoma Cell Line (Caco-2) as a Model System for Intestinal Epithelial Permeability*, *Gastroenterology*, 96 (3), 736-749, 1989.
- 7 Lim, J. Y., A. D. Dreiss, Z. Zhou, J. C. Hansen, C. A. Siedlecki, R. W. Hengstebeck, J. Cheng, N. Winograd, H. J. Donahue, *The Regulation of Integrin-Mediated Osteoblast Focal Adhesion and Focal Adhesion Kinase Expression by Nanoscale Topography*, *Biomaterials*, 28 (10), 1787-1797, 2007.
- 8 Sardella, E., F. Intranuovo, P. Rossini, M. Nardulli, R. Gristina, R. d'Agostino, P. Ravia, *Plasma Enhanced Chemical Vapour Deposition of Nanostructured Fluorocarbon Surfaces*, *Plasma Process Polym*, 6 (S1), 57-60, 2009.
- 9 Cooper, A., S. Jana, N. Bhattarai, M. Zhang, *Aligned Chitosan-Based Nanofibers for Enhanced Myogenesis*, *J Mater Chem*, 20 (40), 8904-8911, 2010.
- 10 Lim, S. H., X. Y. Liu, H. Song, K. J. Yerema, H. Mao, *The Effect of Nanofiber-Guided Cell Alignment on the Preferential Differentiation of Neural Stem Cells*, *Biomaterials*, 31 (34), 9031-9039, 2010.
- 11 Pins, G. D., M. Toner, J. R. Morgan, *Microfabrication of an Analog of the Basal Lamina: Biocompatible Membranes with Complex Topography*, *FASEB J*, 14 (3), 593-602, 2000.

- 12 Jin, C. Y., B. S. Zhu, X. F. Wang, Q. H. Lu, W. T. Chen, X. J. Zhou, *Nanoscale Surface Topography Enhances Cell Adhesion and Gene Expression of Madine Darby Canine Kidney Cells*, *J Mater Sci Mater Med*, 19 (5), 2215-2222, 2008.
- 13 Wang, L., S. K. Murthy, W. H. Fowle, G. A. Barabino, R. L. Carrier, *Influence of Micro-Well Biomimetic Topography on Intestinal Epithelial Caco-2 Cell Phenotype*, *Biomaterials*, 30 (36), 6825-6834, 2009.
- 14 Scheinder, G. B., H. Perinpanayagam, M. Clegg, R. Zaharias, D. Seabold, J. Keller, C. Stanford, *Implant Surface Roughness Affects Osteoblast Gene Expression*, *J Dent Res*, 82 (5), 372-376, 2003.
- 15 Kemkemer, R., C. Neidlinger-Wilke, L. Claes, H. Gruler, *Cell Orientation Induced by Extracellular Signals*, *Cell Biochem Biophys*, 30 (2), 167-192, 1999.
- 16 Schindler, M., I. Ahmed, J. Kamal, A. Nur-E-Kamal, T. H. Grafe, H. Young Chung, S. Meiners, *A Synthetic Nanofibrillar Matrix Promotes in vivo-like Organization and Morphogenesis for Cells in Culture*, *Biomaterials*, 26 (28), 5624-5631, 2005.
- 17 Ott, H., T. S. Matthiesen, S. Goh, L. D. Black, S. M. Kren, T. I. Netoff, D. A. Taylor, *Perfusion-Decellularized Matrix: Using Nature's Platform to Engineer a Bioartificial Heart*, *Nat Med*, 14 (2), 213-221, 2008.
- 18 Hudson, T. W., S. Zawko, C. Deister, S. Lundy, C. Y. Hu, K. Lee, C. E. Schmidt, *Optimized Acellular Nerve Graft is Immunologically Tolerated and Supports Regeneration*, *Tissue Eng*, 10 (11/12), 1641-1651, 2004.
- 19 Pryce Lewis, H. G., K. K. S. Lau, Y. Mao, K. K. Gleason, *Initiated Chemical Vapor Deposition (iCVD) of Polymer Thin Films*, Denver, CO, Annual Technical Conference Proceedings – Society of Vacuum Coaters, 2005.
- 20 Alf, M. E., A. Asatekin, M. C. Barr, S. H. baxamusa, H. Chelawat, G. Ozaydin-Ince, C. D. Petruczuk, R. Sreenivasan, W. E. Tenhaeff, N. J. Trujillo, S. Vaddiraju, J. Xu, K. K. Gleason, *Chemical Vapor Deposition of Conformal, Functional, and Responsive Polymer Films*, *Adv Mater*, 22 (18), 1993-2027, 2010.

- 21 Ertel, S. I., B. D. Ratner, T. A. Horbett, *Radiofrequency Plasma Deposition of Oxygen-Containing Films on poly(ethylene terephthalate) Substrates Improves Endothelial Cell Growth*, J Biomed Mater Res, 24 (12), 1637-1659, 1990.
- 22 Murthy, S. K., B. D. Olsen, K. K. Gleason, *Chemical Vapor Deposition of Fluorocarbon-Organosilicon Copolymers as Biopassivation Coatings for Neural Prostheses*, Indianapolis, IN, Annual Meeting – American Institute of Chemical Engineers, 2002.
- 23 Curtis, A. S., *The Mechanism of Adhesion of Cells to Glass. A Study by Interference Reflection Microscopy*, J Cell Biol, 20, 199-215, 1964.
- 24 Tilghm, R. W., J. T. Parsons, *Focal Adhesion Kinase as a Regulator of Cell Tension in the Progression of Cancer*, Semin Cancer Biol, 18 (1), 45-52, 2008.
- 25 Heydarkhan-Hagvall, S., C. Choi, H. Dunn, S. Heydarkhan, K. Schenke-Layland, W. R. MacLellan, R. E. Beygui, *Influence of Systematically Varied Nano-Scale Topography on Cell Morphology and Adhesion*, Cell Commun Adhes, 14 (5), 181-194, 2008.
- 26 Ng, C. K. M., W. L. Poon, W. Y. Li, T. Cheung, S. H. Cheng, K. N. Yu, *Study of Substrate Topographical Effects on Epithelial Cell Behavior Using Etched Alpha-Particle Tracks on PADC Films*, Nucl Instrum Methods Phys Res B, 266 (14), 3247-3256, 2008.
- 27 Dalby, M. J., M. O. Riehle, S. J. Yarwood, C. D. Wilkinson, A. S. G. Curtis, *Nucleus Alignment and Cell Signaling in Fibroblasts: Response to a Micro-Grooved Topography*, Exp Cell Res, 284 (2), 274-282, 2003.
- 28 Dalby, M. J., M. J. P. Manus, N. Gadegaard, G. Kalna, C. D. W. Wilkinson, A. S. G. Curtis, *Nanotopographical Stimulation of Mechanotransduction and Change in Interphase Centromere Positioning*, J Cell Biochem, 100 (2), 326-338, 2007.
- 29 Ghibado, M., L. Trichet, J. Le Digabel, A. Richert, P. Hersen, B. Ladoux, *Substrate Topography Induces a Crossover from 2D to 3D Behavior in Fibroblast Migration*, Biophys J, 97 (1), 357-368, 2009.
- 30 Biggs, M. J. P., R. G. Richards, S. McFarlane, C. D. W. Wilkinson, R. O. C. Oreffo, M. J. Dalby, *Adhesion Formation of Primary Human Osteoblasts and the Functional Response of Mesenchymal Stem Cells to 330 nm Deep Microgrooves*, J R Soc Interface, 5 (27), 1231-1242, 2008.

- 31 Taylor, M. P., P. L. Timms, G. C. Allen, S. R. Church, *Formation of Oxide Thin Films from Reactions of Hydrogen Peroxide Vapor with Gas Mixtures Containing Silane and Other Hydrides*, *J Mater Chem*, 8 (8), 1769-1771, 1997.
- 32 Cook, G., P. L. Timms, C. Goltner-Spickermann, *Exact Replication of Biological Structures by Chemical Vapor Deposition of Silica*, *Angew Chem Int Ed Engl*, 42 (5), 557-559, 2003.
- 33 Tarducci, C., W. C. E. Schofield, J. P. S. Badyal, S. A. Brewer, C. Willis, *Monomolecular Functionalization of Pulsed Plasma Deposited poly(2-hydroxyethyl methacrylate) Surfaces*, *Chem Mater*, 14 (6), 2541-2545, 2002.
- 34 Pfluger, C. A., R. L. Carrier, B. Sun, K. S. Ziemer, D. D. Burkey, *Cross-Linking and Degradation Properties of Plasma Enhanced Chemical Vapor Deposited poly(2-hydroxyethyl methacrylate)*, *Macromol Rapid Commun*, 30 (2), 126-132, 2009.
- 35 Pfluger, C. A., D. D. Burkey, L. Wang, B. Sun, K. S. Ziemer, R. L. Carrier, *Biocompatibility of Plasma Enhanced Chemical Vapor Deposited poly(2-hydroxyethyl methacrylate) Films for Biomimetic Replication of the Intestinal Basement Membrane*, *Biomacromolecules*, 11 (6), 1579-1584, 2010.
- 36 Chan, K., K. K. Gleason, *Initiated Chemical Vapor Deposition of Linear and Cross-Linked poly(2-hydroxyethyl methacrylate) for Use as Thin-Film Hydrogels*, *Lanmuir*, 21 (19), 8930-8939, 2005.
- 37 Baxamusa, S. H., L. Montero, J. M. Dubach, H. A. Clark, S. Borros, K. K. Gleason, *Protection of Sensors for Biological Applications by Photoinitiated Chemical Vapor Deposition of Hydrogel Thin Films*, *Biomacromolecules*, 9 (10), 2857-2862, 2008.
- 38 Burkey, D. D., K. K. Gleason, *Temperature-Resolved Fourier Transform Infrared Study of Condensation Reactions and Porogen Decomposition in Hybrid Organosilicon-Porogen Films*, *J Vac Sci Technol A*, 22 (1), 61-70, 2004.
- 39 Gunzler, H., H. Gremlich, *IR Spectroscopy: An Introduction*, Wiley-VCH, Weinheim, Germany, 2002.
- 40 Burkey, D. D., K. K. Gleason, *Temperature-Resolved Fourier Transform Infrared Study of Condensation Reactions and Porogen Decomposition in Hybrid Organosilicon-Porogen Films*, *J Vac Sci Technol A*, 22 (1), 61-70, 2004.
- 41 Bosch, S., J. Perez, A. Canillas, *Numerical Algorithm for Spectroscopic Ellipsometry of Thick Transparent Films*, *Appl Opt*, 37 (7), 1177-1179, 1998.

- 42 Beamson, G., High Resolution XPS of Organic Polymers: The Scienta ESCA300 database., Wiley, Chichester, West Sussex, England, 1992.
- 43 Abrahamson, E. W., J. G. F. Littler, K.-P. Vo, *Spectroscopic Basis of Carbonyl Photochemistry. I. The Role of Excited-State Geometry in the Photodecomposition of Formaldehyde*, J Chem Phys, 44 (11), 4082-4086, 1966.